Check for updates

Reinvestigation of Passerini and Ugi scaffolds as multistep apoptotic inducers *via* dual modulation of caspase 3/7 and P53-MDM2 signaling for halting breast cancer†

Mohammed Salah Ayoup,*[a] Yasmin Wahby,[a] Hamida Abdel-Hamid,[a] Marwa M. Abu-Serie,[b] Sherif Ramadan, [cd] Assem Barakat, *[e] Mohamed Teleb[f] and Magda M. F. Ismail[g]

Selective induction of breast cancer apoptosis is viewed as the mainstay of various ongoing oncology drug discovery programs. Passerini scaffolds have been recently exploited as selective apoptosis inducers *via* a caspase 3/7 dependent pathway. Herein, the optimized Passerini caspase activators were manipulated to synergistically induce P53-dependent apoptosis *via* modulating the closely related P53-MDM2 signaling axis. The adopted design rationale and synthetic routes relied on mimicking the general thematic features of lead MDM2 inhibitors incorporating multiple aromatic rings. Accordingly, the cyclization of representative Passerini derivatives and related Ugi compounds into the corresponding diphenylimidazolidine and spiro derivative was performed, resembling the nutlin-based and spiro MDM-2 inhibitors, respectively. The study was also extended to explore the apoptotic induction capacity of the scaffold after simplification and modifications. MTT assay on MCF-7 and MDA-MB231 breast cancer cells compared to normal fibroblasts (WI-38) revealed their promising cytotoxic activities. The flexible Ugi derivatives **3** and **4**, cyclic analog **8**, Passerini adduct **12**, and the thiosemicarbazide derivative **17** were identified as the study hits regarding cytotoxic potency and selectivity, being over 10-folds more potent ($IC_{50} = 0.065-0.096$ μM) and safer (SI = 4.4–18.7) than doxorubicin ($IC_{50} = 0.478$ μM, SI = 0.569) on MCF-7 cells. They promoted apoptosis induction *via* caspase 3/7 activation (3.1–4.1 folds) and P53 induction (up to 4 folds). Further apoptosis studies revealed that these compounds enhanced gene expression of BAX by 2 folds and suppressed Bcl-2 expression by 4.29–7.75 folds in the treated MCF-7 cells. Docking simulations displayed their plausible binding modes with the molecular targets and highlighted their structural determinants of activities for further optimization studies. Finally, *in silico* prediction of the entire library was computationally performed, showing that most of them could be envisioned as drug-like candidates.

[a]*Chemistry Department, Faculty of Science, Alexandria University, P. O. Box 426, Alexandria, 21321, Egypt. E-mail: mohammedsalahayoup@gmail.com; Mohamed.salah@alexu.edu.eg*

[b]*Medical Biotechnology Department, Genetic Engineering and Biotechnology Research Institute, City of Scientific Research and Technological Applications (SRTA-City), Egypt*

[c]*Chemistry Department, Michigan State University, East Lansing, MI 48824, USA*

[d]*Department of Chemistry, Benha University, Benha, Egypt*

[e]*Department of Chemistry, College of Science, King Saud University, P. O. Box 2455, Riyadh 11451, Saudi Arabia. E-mail: ambarakat@ksu.edu.sa*

[f]*Department of Pharmaceutical Chemistry, Faculty of Pharmacy, Alexandria University, Alexandria, 21521, Egypt*

[g]*Department of Pharmaceutical Medicinal Chemistry, Faculty of Pharmacy (Girls), Al-Azhar University, Cairo, 11754, Egypt*

† Electronic supplementary information (ESI) available. See DOI: https://doi.org/10.1039/d3ra04029a

1. Introduction

Breast cancer is the most recognized cancer among women as the universal cause of death. The high incidence and mortality rate of breast cancer have promptly increased, requiring effective treatment protocols.[1] One of the fundamental paths to breast cancer treatment is chemotherapeutic agents; nonetheless, their efficacy for therapeutic control of cancer is extremely restricted by multidrug resistance (MDR), where cancer cells gain resistance, and several cases deteriorate in the first five years.[2–7] Deregulations of apoptosis is regarded as a central aspect that empowers cancer cells to develop MDR; thus, apoptosis induction is a critical approach for breast cancer control and therapy.

Apoptosis evidently requires solid control *via* two proteins: the family of caspase enzymes and inhibitors of

apoptosis proteins (IAPs). Concerning the caspase family, there are two main strategies for apoptosis induction by caspases; the first one is by activation of the mitochondrial apoptotic pathway as an intrinsic pathway and the second strategy commits the activation of an extrinsic pathway (transmembrane-apoptotic pathway).[8,9] Afterwards, both tracks assemble at the effective level of caspases; in the extrinsic pathway, caspases 8 and 10 are engaged, whereas caspases 9 and 2 are involved in the intrinsic pathway. Eventually, apoptosis is initiated by executioner caspases 3 and 7 as feedback to stimuli from both paths.[10] Bcl-2 family proteins and their regulator, the tumor suppressor P53, are adopted in the intrinsic pathway of apoptosis. P53, the "guardian of the genome", is a transcription factor regulating several pivotal genes controlling apoptosis.[11,12] It primarily uses pro-apoptotic proteins to initiate the apoptotic cascade activation[13] and consequent inhibition of the proteins of the mitochondrial anti-apoptotic family, such as Bcl-2.[14,15] Altough P53 activation induces caspase-independent apoptosis,[16] cell senescence, and associated opsonization signal,[17] P53 signals can also promote caspase activation through mitochondrial cytochrome c release.[18] The transcriptional activity of P53 and its levels are tightly controlled by the E3 ubiquitin protein ligase MDM2 that can directly conceal P53 N-terminal transactivation domain,[19] inducing its proteasomal degradation.[20–22] Consistent with its role, MDM2 is viewed as an oncogen when overexpressed.[23] These findings have been mirrored by continuous medicinal chemistry research for drugging these signalling pathways towards efficient anticancer protocols[24–30] Based on the fact that the activity of mature caspases is abrogated by IAPs that are intrinsically inactivated by the secondary mitochondria-derived activator of caspases (SMAC).[31] A tetrapeptide motif of SMAC was viewed as the early lead for designing peptido-mimetic apoptotic inducers. Successive optimization studies led to a series of capped tripeptides[32] and small-molecule caspase activators,[25] of which some reached preclinical evaluation.[26–30] Further fragment-based design protocols identified fragment-derived nonpeptidic clinical-stage apoptotic inducers based on amide core as an essential motif.[33] Recently, our group has developed series of tumor-selective amide-based caspase activators via Passerini multicomponent reaction mimicking the structural features of lead caspase-dependent apoptotic inducers.[34]

On the other hand, substantial investment in direct MDM2 inhibition[35] led to the discovery of nearly twenty different classes of highly potent small-molecule MDM2 inhibitors, of which several efficacious inhibitors have been raised to clinical trials on various human cancers[36–44] including spirooxindoles developed by Sanofi-Aventis (SAR405838),[45] Hoffmann-La Roche (RO2468),[46] and Daiichi Sankyo (DS-3032b)[47] in addition to dozens of leads and active molecules.[48] Nutlins based on imidazoline scaffold have also been investigated by both academic and industrial groups.[48] Clinical studies revealed that combinations of P53 inducers and other agents acting on related signalling pathways, such as Bcl-2 functions, can synergistically promote apoptosis and sensitize the tumor

cells.[49,50] Inspired by these outcomes, we speculated that the next frontier towards efficient apoptotic inducers is to combine the apoptotic induction potential of direct caspase activation and P53-MDM2 axis inhibition for efficient tumor sensitization.

2. Rationale design

The privileged Passerini and related Ugi scaffolds sparked our interest, given their facile synthesis, ease of structure diversification, chemical stability, and efficiency as caspase-dependent apoptotic inducers.[34,51] Accordingly, in continuation of our previous optimization studies of tumor-selective Passerini-based caspase activators,[34,51] we set our design protocol to reinvestigate the potential of these scaffolds to modulate the P53-MDM2 axis. This rationale was considered based on mimicking the general thematic features of MDM2 inhibitors incorporating multiple aromatic rings. Utilizing the optimized tumor-selective Passerini scaffold (Fig. 1), a library of new Passerini and Ugi derivatives with versatile substituents influencing the scaffolds' electronic environment and spatial arrangement was designed and synthesized to allow us to perform structure–activity relationship study. As part of our proposed mimicry design approach, we introduced various functionalities that conferred promising caspase-mediated antitumor activities to lead compounds, especially sulfon-amide,[52] nitro,[53] and azido[54] groups. Moreover, these substituents imparted high potency to our previously reported Passerini[51] and Ugi[55] caspase activators. On the other hand, these functionalities were also represented in several efficient P53 activators, e.g., nonpeptidic sulfonamide P53-MdM2 interaction inhibitors,[56] and nitro-substituted spirooxindoles.[21] A special focus was placed on the designed scaffold flexibility versus the relatively constrained nutlins (I) ((4S,5R)-2,4,5-triphenyl-4,5-dihydro-1H-imidazole) and spirooxindoles ((2'S,3R,4'S,5'R)-6-chloro-4'-(3-chloro-2-fluorophenyl)-N-((1S,3S)-3-hydroxy-3-methylcyclobutyl)-2'-neopentyl-2-oxospiro[indoline-3,3'-pyrrolidine]-5'-carboxamide) (II); thus, the adopted synthetic route involved cyclization of a representative Ugi derivative into the corresponding diphenylimidazolidine derivative (ethyl-4-(2,5-dioxo-3,4-diphenylimidazolidin-1-yl) benzoate) resembling the nutlins (I) family. Similarly, a representative spiro derivative was successfully synthesized from the appropriate Passerini adduct. The study was also extended to probe the effect of scaffold simplification and modifications to enrich the SAR study. The cytotoxicity of our library against the breast cell lines MCF-7 and MDA-MB 231 in comparison to normal human fibroblasts (Wi-38) was examined. Flow cytometric analysis of apoptosis followed by succesive mechanistic apoptosis studies on the promising cytotoxic hits were performed to evaluate their potential to activate caspase 3/7 and modulate P53-MDM2 axis. Other related signalling nodes were also investigated, e.g., Bcl-2 and BAX. Molecular modelling studies were employed to simulate the binding modes of the active compounds within their molecular targets. Finally, brief in silico studies were performed to predict their drug-like candidate properties.
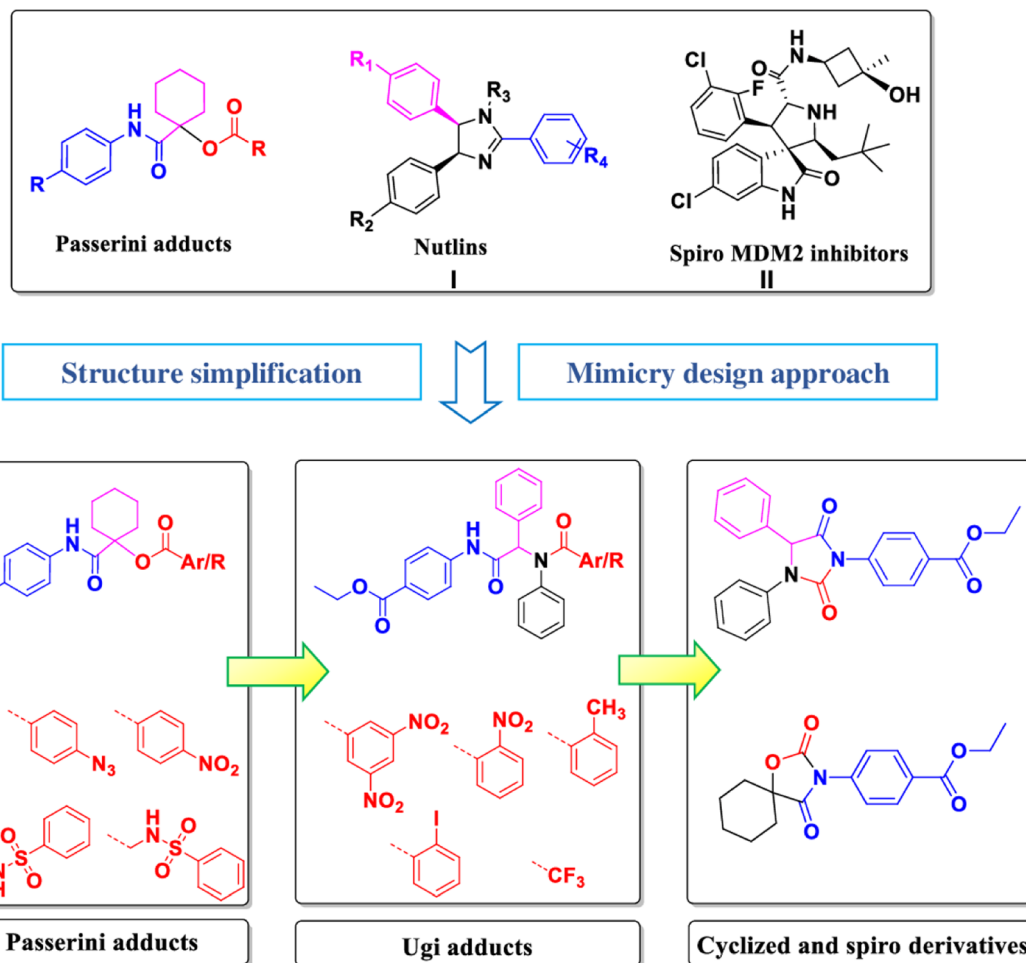
Fig. 1 Target adducts and their derivatives.

3. Materials and methods

3.1. Chemistry

The materials and equipment are described in the ESI.†

3.1.1. General method for Ugi reaction. Aldehyde (0.57 mmol), amine (0.57 mmol), carboxylic acid (0.57 mmol), and ethyl-4-isocyanobenzoate **1** (100 mg, 0.57 mmol) were mixed and dissolved in 3 ml mixture of TFE/EtOH (1 : 1). The stirred mixture was refluxed for 2 days and was continuously monitored by TLC using *n*-hexane/ethyl acetate (2 : 1) as an eluent. Then, the reaction mixture was neutralized with a saturated solution of NaHCO$_3$, followed by extraction with EtOAc (3 × 20 ml). The organic layer was separated, dried over anhydrous Na$_2$SO$_4$, and loaded to column chromatography (silica gel, *n*-hexane/EtOAc (3 : 1)).[55]

3.1.1.1. Ethyl-4-(-phenyl-2-(2,2,2-trifluoro-N-phenyl-acetamido)acetamido)benzoate (2). Yellow crystals: yield 59%; m.p. = 102–104 °C; R_f 0.4 (2 : 1, *n*-hexane/EtOAc); IR ν_{max}/cm^{-1}: 3314 (–NH), 1690, 1662 (–CO, –NCO); ^{1}H-NMR (500 MHz, DMSO-d_6) δ_H: 10.74 (s, 1H, –**NH**), 7.89 (d, J = 9.0 Hz, 2H, aromatic–**H**), 7.72 (d, J = 8.5 Hz, 3H, aromatic–**H**), 7.32–7.27 (m, 1H, aromatic–**H**), 7.16–7.10 (m, 6H, aromatic–**H**), 6.98 (t, J = 8.0 Hz, 1H, aromatic–**H**), 6.79 (d, J = 8.0 Hz, 1H, aromatic–**H**),

6.14 (s, 1H, *N*–**CH**), 4.24 (q, J = 7.5 Hz, 2H, **CH$_3$**–**CH$_2$O**), 1.26 (t, J = 7.0 Hz, 3H, **CH$_3$**–**CH$_2$O**); ^{13}C-NMR (125 MHz, DMSO-d_6) δ_C: 168.4 (NH–**CO**), 165.8 (EtO–**CO**), 156.5, 156.3 (d, J = 33.3 Hz, N–**CO**–CF$_3$), 143.5, 135.9, 132.2, 131.7, 131.4, 131.3, 130.9, 130.3, 129.5, 129.4, 129.2, 128.7, 128.4, 128.3, 127.6, 125.1, 122.1, 119.1 (aromatic–**C**), 67.0 (*N*–**CH**), 61.0 (**OCH$_2$**), 14.7 (**CH$_3$**). Anal. calc. for C$_{25}$H$_{21}$F$_3$N$_2$O$_4$ (470.45); C, 63.83; H, 4.50; N, 5.95; found: C, 63.73; H, 4.72; N, 6.03.

3.1.1.2. Ethyl-4-(2-(2-methyl-N-phenylbenzamido)-2-phenylacetamido)benzoate (3). Pale brown powder: yield 56%; m.p. = 80–82 °C; R_f 0.20 (2 : 1, *n*-hexane/EtOAc); IR ν_{max}/cm^{-1}: 3118 (–NH), 1709 (br, –CO, –NCO); ^{1}H-NMR (500 MHz, DMSO-d_6) δ_H: 10.71 (s, 1H, –**NH**), 7.91 (d, J = 9.0 Hz, 2H, aromatic–**H**), 7.77 (d, J = 9.0 Hz, 2H, aromatic–**H**), 7.13–6.97 (m, 10H, aromatic–**H**), 6.88–6.82 (m, 4H, aromatic–**H**), 6.37 (s, 1H, *N*–**CH**), 4.25 (q, J = 7.0 Hz, 2H, **CH$_3$**–**CH$_2$O**), 2.27 (s, 3H, aromatic–**CH$_3$**), 1.27 (t, J = 7.0 Hz, 3H, **CH$_3$**–**CH$_2$O**); ^{13}C-NMR (125 MHz, DMSO-d_6) δ_C: 171.0 (*N*–**CO**), 170.0 (NH–**CO**), 165.8 (EtO–**CO**), 143.9, 139.6, 137.3, 134.6, 134.3, 131.3, 130.9, 130.2, 128.7, 128.2, 127.6, 127.4, 125.2, 124.8, 119.0 (aromatic–**C**), 65.3 (*N*–**CH**), 61.0 (**OCH$_2$**), 19.6 (aromatic–**CH$_3$**), 14.8 (**OCH$_2$**–**CH$_3$**). Anal. calc. for C$_{31}$H$_{28}$N$_2$O$_4$ (492.58); C, 75.59; H, 5.73; N, 5.69; found: C, 75.73; H, 5.59; N, 5.74.

3.1.1.3. Ethyl-4-(2-(2-iodo-N-phenylbenzamido)-2-phenylacetamido)benzoate (4). Buff powder: yield 67%; m.p. = 130–132 °C; R_f 0.27 (2 : 1, *n*-hexane/EtOAc); IR ν_{max}/cm^{-1}: 3394 (–NH), 1701 (br, –CO, –NCO); ^{1}H-NMR (500 MHz, DMSO-d_6) δ_H: 10.77 (s, 1H, –**NH**), 7.94 (d, *J* = 9.0 Hz, 2H, aromatic–**H**), 7.81 (d, *J* = 8.5 Hz, 2H, aromatic–**H**), 7.65–7.61 (m, 2H, aromatic–**H**), 7.36–7.14 (m, 8H, aromatic–**H**), 7.04–6.86 (m, 4H, aromatic–**H**), 6.42 (s, 1H, *N*–**CH**), 4.28 (q, *J* = 7.0 Hz, 2H, CH₃–**CH₂O**), 1.30 (t, *J* = 7.5 Hz, 3H, **CH₃**–CH₂O); ^{13}C-NMR (125 MHz, DMSO-d_6) δ_C: 169.7 (*N*–**CO**), 169.0 (NH–**CO**), 165.3 (EtO–**CO**), 153.5, 143.3, 142.2, 138.5, 138.4, 133.6, 131.1, 130.4, 130.3, 129.8, 128.4, 128.3, 127.8, 127.6, 127.3, 124.4, 118.6, 112.6 (aromatic–**C**), 94.1 (**C**–I), 64.6 (*N*–**CH**), 60.5 (**OCH₂**), 14.3 (**CH₃**). Anal. calc. for C₃₀H₂₅IN₂O₄ (604.44); C, 59.61; H, 4.17; N, 4.63; found: C, 59.76; H, 4.05; N, 4.69.

3.1.1.4. Ethyl-4-(2-(2-nitro-N-phenylbenzamido)-2-phenylacetamido)benzoate (5). Green crystals: yield 70%; m.p. = 193–195 °C; R_f 0.29 (2 : 1, *n*-hexane/EtOAc); IR ν_{max}/cm^{-1}: 3327 (–NH), 1719 (br, –CO, –NCO); ^{1}H-NMR (500 MHz, DMSO-d_6) δ_H: 10.79 (s, 1H, –**NH**), 7.92 (dd, *J* = 8.0, 1.5 Hz, 3H, aromatic–**H**), 7.78 (d, *J* = 8.5 Hz, 2H, aromatic–**H**), 7.58 (t, *J* = 8.5 Hz, 1H, aromatic–**H**), 7.43–7.39 (m, 2H, aromatic–**H**), 7.15 (t, *J* = 4.0 Hz, 6H, aromatic–**H**), 6.89 (bs, 3H, aromatic–**H**), 6.44 (s, 1H, *N*–**CH**), 4.25 (q, *J* = 7.0 Hz, 2H, CH₃–**CH₂O**), 1.27 (t, *J* = 7.0 Hz, 3H, **CH₃**–CH₂O); ^{13}C-NMR (125 MHz, DMSO-d_6) δ_C: 168.8 (*N*–**CO**), 166.9 (NH–**CO**), 165.3 (EtO–**CO**), 144.9, 143.2, 138.3, 134.2, 133.4, 132.5, 130.6, 130.4, 130.3, 130.1, 129.4, 128.4, 128.3, 128.1, 127.8, 124.4, 124.1, 118.6 (aromatic–**C**), 64.6 (*N*–**CH**), 60.5 (**OCH₂**), 14.2 (**CH₃**). Anal. calc. for C₃₀H₂₅N₃O₆ (523.55); C, 68.83; H, 4.81; N, 8.03; found: C, 68.95; H, 4.77; N, 8.10.

3.1.1.5. Ethyl-4-(2-(3,5-dinitro-N-phenylbenzamido)-2-phenylacetamido)benzoate (6). Orange powder: yield 60%; m.p. = 170–172 °C; R_f 0.19 (2 : 1, *n*-hexane/EtOAc); IR ν_{max}/cm^{-1}: 3328 (–NH), 1709 (br, –CO, –NCO); ^{1}H-NMR (500 MHz, DMSO-d_6) δ_H: 10.80 (s, 1H, –**NH**), 8.63 (t, *J* = 2.0 Hz, 1H, aromatic–**H**), 8.36 (d, *J* = 1.5 Hz, 2H, aromatic–**H**), 7.91 (d, *J* = 9.0 Hz, 2H, aromatic–**H**), 7.78 (d, *J* = 8.5 Hz, 2H, aromatic–**H**), 7.21–7.14 (m, 6H, aromatic–**H**), 7.01–6.93 (m, 4H, aromatic–**H**), 6.42 (s, 1H, *N*–**CH**), 4.25 (q, *J* = 7.5 Hz, 2H, CH₃–**CH₂O**), 1.27 (t, *J* = 7.0 Hz, 3H, **CH₃**–CH₂O); ^{13}C-NMR (125 MHz, DMSO-d_6) δ_C: 169.4 (*N*–**CO**), 166.2 (NH–**CO**), 165.8 (EtO–**CO**), 147.9, 143.7, 139.5, 139.3, 133.7, 131.6, 131.0, 130.9, 129.0, 128.9, 128.8, 128.7, 128.4, 125.0, 119.8, 119.2 (aromatic–**C**), 65.9 (*N*–**CH**), 61.0 (**OCH₂**), 14.7 (**CH₃**). Anal. calc. for C₃₀H₂₄N₄O₈ (568.16); C, 63.38; H, 4.26; N, 9.85; found: C, 63.16; H, 4.18; N, 9.91.

3.1.1.6. Ethyl-4-(2,5-dioxo-3,4-diphenylimidazolidin-1-yl) benzoate (8). Off-white powder: yield 58%; m.p. = 62–64 °C; R_f 0.48 (2 : 1, *n*-hexane/EtOAc); IR ν_{max}/cm^{-1}: 1779 (–CO), 1724 (CO–N–CO); ^{1}H-NMR (500 MHz, DMSO-d_6) δ_H: 8.07 (d, *J* = 8.5, 2H, aromatic–**H**), 7.64 (d, *J* = 8.5 Hz, 2H, aromatic–**H**), 7.54 (d, *J* = 8.0 Hz, 2H, aromatic–**H**), 7.49 (d, *J* = 7.5 Hz, 2H, aromatic–**H**), 7.34–7.28 (m, 5H, aromatic–**H**), 7.07 (t, *J* = 7.0 Hz, 1H, aromatic–**H**), 6.12 (s, 1H, *N*–**CH**), 4.30 (q, *J* = 7.5 Hz, 2H, CH₃–**CH₂O**), 1.30 (t, *J* = 7.5 Hz, 3H, **CH₃**–CH₂O); ^{13}C-NMR (125 MHz, DMSO-d_6) δ_C: 169.8 (*N*–**CO**–CH), 165.6 (EtO–**CO**), 153.4 (*N*–**CO**–N), 136.6, 136.4, 134.1, 130.3, 129.8, 129.5, 129.4, 128.3, 127.6, 125.4,

122.1, 64.0 (*N*–**CH**), 61.6 (**OCH₂**), 14.7 (**CH₃**). Anal. calc. for C₂₄H₂₀N₂O₄ (400.43); C, 71.99; H, 5.03; N, 7.00; found: C, 72.13; H, 5.11; N, 7.08.

3.1.2. General method for Passerini reaction. Ethyl-4-isocyanobenzoate **1** (50 mg, 0.286 mmol, 0.5 eq.), cyclohexanone (2.86 mmol, 5 eq.), and carboxylic acids (0.57 mmol, 1 eq.) were placed in a dry flask. The reaction mixture was stirred for 24 h at room temperature. The reaction progress was monitored by TLC using *n*-hexane/ethyl acetate (2 : 1) as an eluent. Then, the reaction was quenched by adding 5 ml of dichloromethane and neutralized by NaHCO₃ saturated solution. The organic layer was separated, dried over anhydrous Na₂SO₄, and loaded to column chromatography for purification.[34]

3.1.2.1. 1-((4-(Ethoxycarbonyl)phenyl)carbamoyl)cyclohexyl-2-methylbenzoate (9). Off-white powder: yield 50%; m.p. = 121–124 °C; R_f 0.54 (2 : 1, *n*-hexane/EtOAc); IR ν_{max}/cm^{-1}: 3337 (–NH), 1720, 1697 (–CO, –NCO); ^{1}H-NMR (500 MHz, DMSO-d_6) δ_H: 9.98 (s, 1H, –**NH**), 7.95 (d, *J* = 7.5 Hz, 1H, aromatic–**H**), 7.88 (d, *J* = 8.0 Hz, 2H, aromatic–**H**), 7.78 (d, *J* = 9.0 Hz, 2H, aromatic–**H**), 7.50 (t, *J* = 6.0 Hz, 1H, aromatic–**H**), 7.38–7.32 (m, 2H, aromatic–**H**), 4.26 (q, *J* = 7.0 Hz, 2H, CH₃–**CH₂O**), 2.41 (s, 3H, **CH₃**–aromatic), 2.29 (d, *J* = 13.5 Hz, 2H, cyclohexylidene–**H**), 1.91–1.85 (td, *J* = 13.5, 3.5 Hz, 2H, cyclohexylidene–**H**), 1.69–1.55 (m, 5H, cyclohexylidene–**H**), 1.34–1.32 (m, 1H, cyclohexylidene–**H**), 1.29 (t, *J* = 7.5 Hz, 3H, **CH₃**–CH₂O); ^{13}C-NMR (125 MHz, DMSO-d_6) δ_C: 171.4 (NH–**CO**), 165.7 (**C**–O–CO), 165.4 (EtO–**CO**), 143.5, 139.3, 132.3, 131.6, 130.2, 130.0, 126.1, 124.4, 119.5 (aromatic–**C**), 81.9 (O=C–**CO**), 60.5 (**OCH₂**), 31.4, 24.6, 21.2, 20.9 (cyclohexylidene–**C**), 14.3 (**CH₃**). Anal. calc. for C₂₄H₂₇NO₅ (409.48); C, 70.40; H, 6.65; N, 3.42; found: C, 70.34; H, 6.57; N, 3.49.

3.1.2.2. 1-((4-(Ethoxycarbonyl)phenyl)carbamoyl)cyclohexyl-4-azidobenzoate (10). Off-white crystals: yield 56%; m.p. = 182–184 °C; R_f 0.74 (2 : 1, *n*-hexane/EtOAc); IR ν_{max}/cm^{-1}: 3319 (–NH), 2125 (–N₃), 1711 (br, –CO, –NCO); ^{1}H-NMR (500 MHz, DMSO-d_6) δ_H: 9.94 (s, 1H, –**NH**), 8.02 (d, *J* = 8.5 Hz, 2H, aromatic–**H**), 7.84 (d, *J* = 8.5, 2H, aromatic–**H**), 7.72 (d, *J* = 8.5 Hz, 2H, aromatic–**H**), 7.25 (d, *J* = 8.5 Hz, 2H, aromatic–**H**), 4.23 (q, *J* = 7.0 Hz, 2H, CH₃–**CH₂O**), 2.27 (d, *J* = 13.5 Hz, 2H, cyclohexylidene–**H**), 1.84 (td, *J* = 13.5, 3.0 Hz, 2H, cyclohexylidene–**H**), 1.64 (d, *J* = 10.0 Hz, 3H, cyclohexylidene–**H**), 1.55–1.48 (m, 2H, cyclohexylidene–**H**), 1.33–1.30 (m, 1H, cyclohexylidene–**H**), 1.26 (t, *J* = 7.0 Hz, 3H, **CH₃**–CH₂O); ^{13}C-NMR (125 MHz, DMSO-d_6) δ_C: 171.8 (NH–**CO**), 165.9 (**C**–O–CO), 164.2 (EtO–**CO**), 145.2, 143.9, 132.1, 130.4, 126.8, 124.9, 120.1, 119.9 (aromatic–**C**), 82.2 (O=C–**CO**), 61.0 (**OCH₂**), 31.9, 25.1, 21.6 (cyclohexylidene–**C**), 14.7 (**CH₃**). Anal. calc. for C₂₃H₂₄N₄O₅ (436.47); C, 63.29; H, 5.54; N, 12.84; found: C, 63.17; H, 5.59; N, 12.77.

3.1.2.3. 1-((4-(Ethoxycarbonyl)phenyl)carbamoyl)cyclohexyl 4-nitrobenzoate (11). Off-white crystals: yield 51%; m.p. = 239–241 °C; R_f 0.58 (2 : 1, *n*-hexane/EtOAc); IR ν_{max}/cm^{-1}: 3328 (–NH), 1714 (br, –CO, –NCO); ^{1}H-NMR (500 MHz, DMSO-d_6) δ_H: 9.99 (s, 1H, –**NH**), 8.36 (d, *J* = 7.5 Hz, 2H, aromatic–**H**), 8.25 (d, *J* = 7.5 Hz, 2H, aromatic–**H**), 7.85 (d, *J* = 8.0 Hz, 2H, aromatic–**H**), 7.72 (d, *J* = 7.5 Hz, 2H, aromatic–**H**), 4.23 (q, *J* = 6.0 Hz, 2H, CH₃–**CH₂O**), 2.29 (d, *J* = 14.0 Hz, 2H, cyclohexylidene–**H**), 1.90 (t, *J* = 12.5 Hz, 2H, cyclohexylidene–**H**), 1.65 (bs, 3H,

cyclohexylidene–**H**), 1.58–1.51 (m, 2H, cyclohexylidene–**H**), 1.40–1.31 (m, 1H, cyclohexylidene–**H**), 1.26 (t, J = 7.0 Hz, 3H, **CH₃**–CH₂O); ¹³C-NMR (125 MHz, DMSO-d_6) δ_C: 171.3 (NH–CO), 165.8 (C–O–CO), 163.5 (EtO–CO), 150.9, 143.7, 135.7, 131.6, 130.5, 125.0, 124.5, 120.2 (aromatic–C), 83.3 (O=C–CO), 61.0 (OCH₂), 31.9, 25.0, 21.6 (cyclohexylidene–C), 14.7 (**CH₃**). Anal. calc. for C₂₃H₂₄N₂O₇ (440.45); C, 62.72; H, 5.49; N, 6.36; found: C, 62.85; H, 5.42; N, 6.22.

3.1.2.4. 1-((4-(Ethoxycarbonyl)phenyl)carbamoyl)cyclohexyl-4-(phenylsulfonamido)benzoate (12). Yellow powder: yield 45%; m.p. = 220–222 °C; R_f 0.56 (2 : 1, n-hexane/EtOAc); IR ν_{max}/cm⁻¹: 3404 (–NH), 1717, 1669 (–CO, –NCO); ¹H-NMR (500 MHz, DMSO-d_6) δ_H: 10.93, 9.86 (s, 2H, 2**NH**'s), 7.87–7.81 (m, 6H, aromatic–**H**), 7.69 (d, J = 8.0 Hz, 2H, aromatic–**H**), 7.62–7.53 (m, 3H, aromatic–**H**), 7.22 (d, J = 8.5 Hz, 2H, aromatic–**H**), 4.22 (q, J = 7.0 Hz, 2H, CH₃–**CH₂**O), 2.20 (d, J = 13.0 Hz, 2H, cyclohexylidene–**H**), 1.79 (t, J = 11.5 Hz, 2H, cyclohexylidene–**H**), 1.61–1.48 (m, 5H, cyclohexylidene–**H**), 1.27 (t, J = 7.0 Hz, 3H, **CH₃**–CH₂O), 1.19 (s, 1H, cyclohexylidene–**H**); ¹³C-NMR (125 MHz, DMSO-d_6) δ_C: 171.9 (NH–CO), 165.9 (C–O–CO), 164.4 (EtO–CO), 143.9, 143.4, 139.8, 133.8, 131.6, 130.4, 130.0, 127.2, 124.9, 124.8, 120.1, 118.5 (aromatic–C), 81.9 (O=C–CO), 61.0 (OCH₂), 31.9, 25.1, 21.6 (cyclohexylidene–C), 14.7 (**CH₃**). Anal. calc. for C₂₉H₃₀N₂O₇S (550.63); C, 63.26; H, 5.49; N, 5.09; S, 5.82; found: C, 63.14; H, 5.17; N, 5.03; S, 5.75.

3.1.2.5. Ethyl 4-(1-(2-(phenylsulfonamido)acetoxy)cyclohexanecarboxamido)benzoate (13). White powder: yield 49%; m.p. = 198–199 °C; R_f 0.23 (2 : 1, n-hexane/EtOAc); IR ν_{max}/cm⁻¹: 3228 (–NH), 1757, 1702 (–CO, –NCO); ¹H-NMR (500 MHz, DMSO-d_6) δ_H: 9.76 (s, 1H, –**NH**), 8.22 (t, J = 6.5 Hz, 1H, CH₂–**NH**), 7.85 (d, J = 9.0 Hz, 2H, aromatic–**H**), 7.73–7.68 (m, 4H, aromatic–**H**), 7.55–7.52 (m, 1H, aromatic–**H**), 7.44 (t, J = 8.0 Hz, 2H, aromatic–**H**), 4.24 (q, J = 7.5 Hz, 2H, CH₃–**CH₂**O), 3.87 (d, J = 6.5 Hz, 2H, **OCH₂**–NH), 1.98 (d, J = 13.0 Hz, 2H, cyclohexylidene–**H**), 1.68 (td, J = 14.5, 4.0 Hz, 2H, cyclohexylidene–**H**), 1.56–1.50 (m, 3H, cyclohexylidene–**H**), 1.44–1.37 (m, 2H, cyclohexylidene–**H**), 1.26 (t, J = 7.0 Hz, 3H, **CH₃**–CH₂O); 1.24 (m, 1H, cyclohexylidene–**H**); ¹³C-NMR (125 MHz, DMSO-d_6) δ_C: 171.4 (NH–CO), 168.3 (C–O–CO), 165.9 (EtO–CO), 143.7, 141.1, 133.0, 130.4, 129.6, 127.0, 125.0, 120.0 (aromatic–C), 82.6 (O=C–CO), 61.0 (OCH₂), 44.4 (CH₂–NH), 31.8, 25.0, 21.2 (cyclohexylidene–C), 14.7 (**CH₃**). Anal. calc. for C₂₄H₂₈N₂O₇S (488.56); C, 59.00; H, 5.78; N, 5.73; S, 6.56; found: C, 59.09; H, 5.81; N, 5.69; S, 6.50.

3.1.2.6. 4-(1-(Carboxyoxy)cyclohexane-1-carboxamido)benzoic acid (15). Ethyl-4-(2,4-dioxo-1-oxa-3-azaspiro[4.5]decan-3-yl) benzoate **14** (0.315 mmol, 1 eq.) and NaOH (0.946 mmol, 3 eq.) were placed in EtOH/H₂O (1 : 1) mixture. The stirred mixture was refluxed for 1 h and was monitored continuously by TLC till reaction completion. After that, the reaction mixture was cooled, acidified till pH = 2 using HCl (2M), the crude product was precipitated, and collected by filtration. Off-white crystals: yield 51%; m.p. = 220–222 °C; R_f 0.54 (2 : 1, n-hexane/EtOAc); IR ν_{max}/cm⁻¹: 3291 (–NH), 1700 (br, –CO, –NCO); ¹H-NMR (500 MHz, DMSO-d_6) δ_H: 12.66 (s, 2H, 2**OH**'s), 10.04 (s, 1H, –**NH**), 7.82 (d, J = 9.0 Hz, 2H, aromatic–**H**), 7.52 (d, J = 8.5 Hz, 2H, aromatic–**H**), 2.07 (d, J = 13.5 Hz, 2H,

cyclohexylidene–**H**), 1.73 (dist.td, J = 14.0, 3.0 Hz, 2H, cyclohexylidene–**H**), 1.57–1.46 (m, 5H, cyclohexylidene–**H**), 1.30–1.22 (m, 1H, cyclohexylidene–**H**); ¹³C-NMR (125 MHz, DMSO-d_6) δ_C: 173.9 (NH–CO), 167.0 (aromatic–CO–OH), 152.1 (O–CO–OH), 143.3, 130.5, 124.4, 117.4 (aromatic–C), 79.2 (O=C–CO), 32.0, 24.7, 21.0 (cyclohexylidene–C). Anal. calc. for C₁₅H₁₇NO₆ (307.30); C, 58.63; H, 5.58; N, 4.56; found: C, 58.77; H, 5.65; N, 4.48.

3.1.2.7. N-(4-(Hydrazinecarbonyl)phenyl-1-hydroxycyclohexane-1-carboxamide (16). 1-((4-(Ethoxycarbonyl)phenyl)carbamoyl) cyclohexyl-4-nitrobenzoate (11) (70 mg, 0.16 mmole) in 2 ml of hydrazine (99%) was refluxed for 2 days and monitored continuously by TLC. The product precipitate is formed after cooling the mixture. The product was filtered and collected without any further purification. Off-white powder: yield 46%; m.p. = 201–204 °C; R_f 0.48 (1 : 1 : 1, n-hexane/EtOAc/methanol); IR ν_{max}/cm⁻¹: 3549 (–OH), 3411, 3332, 3270 (–NH's), 1651 (–NCO); ¹H-NMR (500 MHz, DMSO-d_6) δ_H: 9.76, 9.61 (2s, 2H, 2**NH**'s), 7.82–7.71 (m, 4H, aromatic–**H**), 7.22 (s, 1H, –**NH**), 5.49 (s, 1H, –**OH**), 4.42 (s, 1H, –**NH**), 1.70 (m, 2H, cyclohexylidene–**H**), 1.57–1.47 (m, 7H, cyclohexylidene–**H**), 1.21–1.16 (m, 1H, cyclohexylidene–**H**); ¹³C-NMR (125 MHz, DMSO-d_6) δ_C: 176.9, 167.9 (2NH–CO), 142.0, 141.9, 129.2, 128.7, 128.2, 128.1, 119.3, 119.2 (aromatic–C), 74.5 (O=C–CO), 34.2, 25.5, 21.3 (cyclohexylidene–C). Anal. calcd for C₁₄H₁₉N₃O₃ (277.32): C, 60.63; H, 6.91; N, 15.15; found C, 60.77; H, 6.99; N, 15.08.

3.1.2.8. 1-Hydroxy-N-(4-(2-(phenylcarbamothioyl)hydrazine-1-carbonyl)phenyl)cyclohexane-1-carboxamide (17). A solution of N-(4-(hydrazinecarbonyl)phenyl)-1-hydroxycyclohexane-1-carboxamide **16** (300 mg, 1.08 mmol) and phenyl isothiocyanate (160 mg, 1.19 mmol) in 5 mL absolute ethanol was refluxed for 8 h. The reaction mixture was continuously monitored by TLC till reaction completion. After that, the mixture was cooled at room temperature. The formed solid was collected by filtration and purified using column chromatography. Orange powder: yield 69%; m.p. = 165–168 °C; R_f 0.5 (2 : 1, n-hexane/EtOAc); IR ν_{max}/cm⁻¹: 3346, 3259 (br, –NH's), 1671 (–NCO); ¹H-NMR (500 MHz, DMSO-d_6) δ_H: 10.39, 9.86, 9.65 (3s, 3H, 3**NH**'s), 9.76 (s, 1H, –**NH**), 7.85 (q, J = 9 Hz, 4H, aromatic–**H**), 7.39 (bs, 2H, aromatic–**H**), 7.29 (t, J = 7.5 Hz, 2H, aromatic–**H**), 7.12 (t, J = 6.5 Hz, 1H, aromatic–**H**), 5.51 (s, 1H, –**OH**), 1.71 (td, J = 13.5, 4.5 Hz, 2H, cyclohexylidene–**H**), 1.58–1.48 (m, 7H, cyclohexylidene–**H**), 1.28–1.14 (m, 1H, cyclohexylidene–**H**); ¹³C-NMR (125 MHz, DMSO-d_6) δ_C: 177.0, 166.0 (2NH–CO), 142.6, 139.8, 129.2, 128.4, 127.4, 126.6, 119.1 (aromatic–C), 74.5 (O=C–CO), 34.2, 25.5, 21.3 (cyclohexylidene–C). Anal. calcd for C₂₁H₂₄N₄O₃S (412.51): C, 61.14; H, 5.86; N, 13.58; S, 7.77; found C, 61.22; H, 5.93; N, 13.49; S, 7.83.

3.2. Biological evaluation

3.2.1. Determination of cytotoxicity. The experimental procedure for determining the cytotoxicity is described in the ESI.†

3.2.2. Flow cytometric analysis of apoptosis-mediated anticancer effect. Flow cytometric analysis of apoptosis is described in the ESI.†

3.2.3. Caspase 3/7 activation assay. Caspase 3/7 activation assay is described in the ESI.†

3.2.4. Quantitative detection of P53, Bcl-2, and BAX in the treated cancer cells. The quantitative detection of change in the expression of P53, Bcl-2, and BAX is described in the ESI.†

3.2.5. Molecular modeling studies. Docking simulation procedures are described in the ESI.†

3.2.6. Statistical analysis. Statistical analysis method is described in the ESI.†

# 4. Results and discussion

4.1. Chemistry

Multicomponent reactions (MCRs) are straightforward chemical reactions that include a group of chemical transformations in a single step without the isolation of intermediates.

Ugi-MCR is a one-pot condensation reaction of amines, carboxylic acid derivatives, and isonitriles for the generation of classical bisamide products. The application of the Ugi reaction generates a variety of biologically active molecules, which has attracted attention in recent years.[57–61] Herein, we utilized ethyl-4-isocyanobenzoate (**1**) as an entry to Passerini and Ugi products; it was prepared *via* esterification of 4-aminobenzoic acid to afford the ester; then, formylation using HCOOH/toluene protocol yielded the formamide, which underwent dehydration by Wang's method[62,63] to give the corresponding isonitrile, **1** in good yield.

α-Aminoacyl amides (**2–6**) were prepared *via* Ugi reaction where the interaction occurs between the isonitrile **1**, aniline,

benzaldehyde, and various carboxylic acids (trifluoroacetic acid, *o*-toluic acid, *o*-iodobenzoic acid, *o*-nitrobenzoic acid, and 3,5-dinitrobenzoic acid) using trifluoroethanol/ethanol mixture (1 : 1) under reflux condition (Scheme 1). Ugi structures were confirmed based on IR and NMR spectral data. Their ^{1}H-NMR spectra clearly recorded –**NH** singlet signals between δ_H 10.81 and 10.71 ppm, and the aromatic proton signals appeared at δ_H 6.94–6.79 ppm. Methine protons (*N*–**CH**) of all products were recorded as singlet signals between δ_H 6.44 and 6.14 ppm. Also, protons of **CH$_2$** and **CH$_3$** of the ethyl group appeared in the range δ_H 4.28–4.24 and 1.30–1.26 ppm, respectively. Moreover, the ^{13}C-NMR spectrum showed the carbonyl carbons of bis-amide in all Ugi products resonating from δ_c 171.0 to 156.3 ppm. The aromatic carbon signals were recorded between δ_C 147.9 and 118.6 ppm. Methine carbons (N–**CH**–CO) appeared between δ_C 67.5 and 64.6 ppm. Carbon signals of the carbonyl group of **COCF$_3$** for compound **2** appeared as a doublet at 156.5 and 156.3 ppm with *J* coupling 33.3 Hz. The methyl group (Ar–**CH$_3$**) in product **3** showed signals at δ_C 19.6 ppm. For product **4**, carbon of **C**–I showed a signal recorded at δ_C 94.1 ppm.

Moreover, the synthesis of ethyl 4-(2,5-dioxo-3,4-diphenylimidazolidin-1-yl)benzoate (**8**) was performed using ethyl-4-isocyanobenzoate **1**, aniline, benzaldehyde and trichloroacetic acid under reflux in EtOH/TFE to yield the intermediate **7**. The latter was cyclized immediately *via* intramolecular attack of the nucleophile NH to the electrophilic center of the carbonyl of **COCCl$_3$** to afford the unexpected
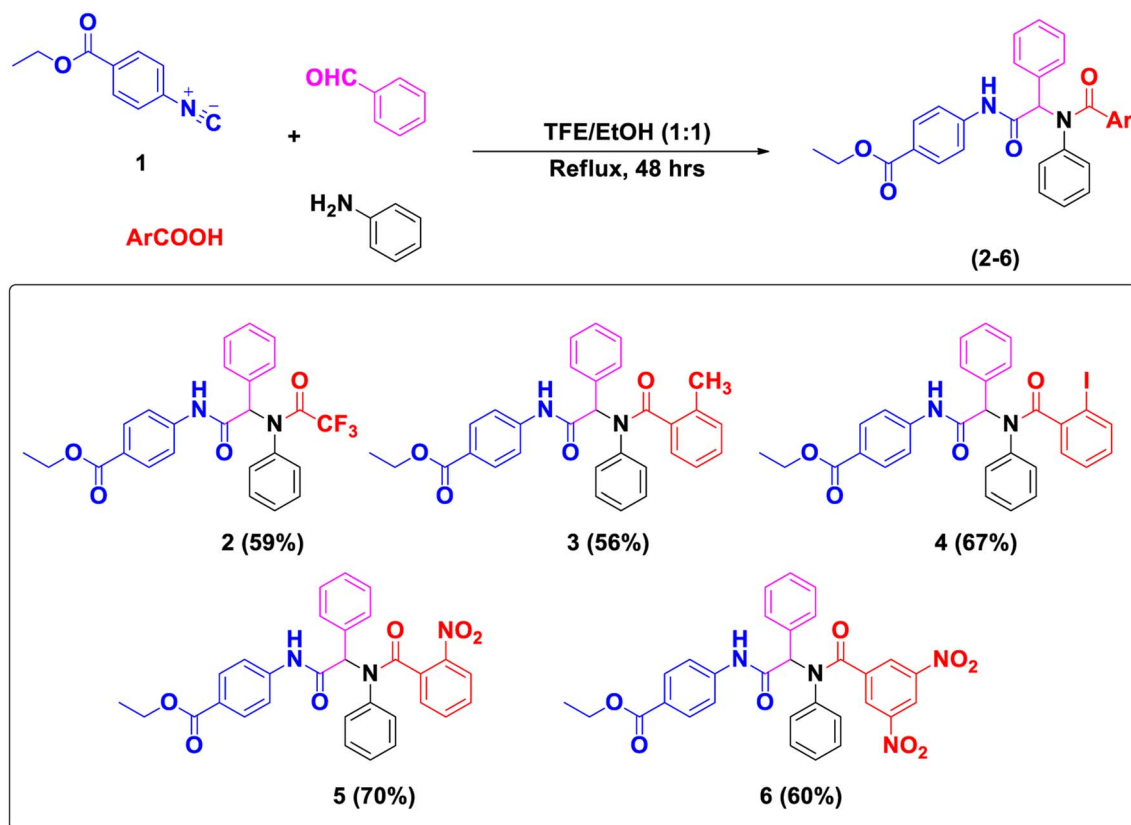
Scheme 1 Synthesis of α-acylamino amide derivatives **2–6** *via* Ugi reaction.
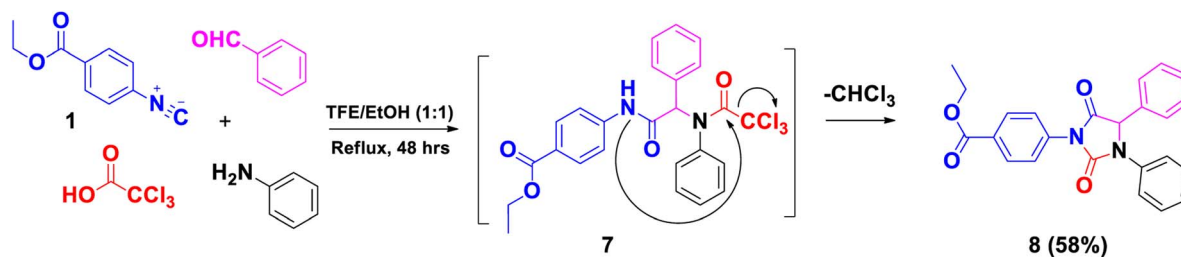
Scheme 2 Synthesis of ethyl 4-(2,5-dioxo-3,4-diphenylimidazolidin-1-yl)benzoate (**8**).

compound **8** with the elimination of one molecule of CHCl$_3$ (Scheme 2). ^{1}H-NMR confirmed the structure of **8**, revealing the lack of –**NH** signal; in addition, methine proton (Ph–**CH**) appeared as a singlet signal at δ_H 6.12 ppm. ^{13}C-NMR showed a methine carbon (Ph–**CH**) signal at δ_C 64.0 ppm and 2 CO signals of oxazolinedione at δ_C 169.8 and 153.4 ppm.

Furthermore, Mario Passerini explored the first multicomponent reaction nearly a century ago. Passerini reactions, in a one-pot fashion,[34] offer great advantages over classical bimolecular reactions. Novel α-acyloxy carboxamides (**9–13**) were synthesized according to the Passerini method by using ethyl-4-isocyanobenzoate **1**, cyclohexanone with miscellaneous carboxylic acids, namely 4-(phenylsulfonamido)benzoic acid, 2-(phenylsulfonamido)acetic acid, o-toluic acid, p-azidobenzoic acid or p-nitrobenzoic acid, at room temperature (Scheme 3). The obtained compounds (**9–13**) were analyzed by FT-IR and NMR spectroscopy. ^{1}H-NMR spectra showed signals from δ_H 9.99–9.76 ppm for –**NH** in amido groups. Protons of aromatic

moiety showed signals at δ_H 7.25–8.36 ppm and c-hexylidene protons (10 Hs) at δ_H 2.29–1.19 ppm. Aliphatic protons of –OCH$_2$ and –CH$_3$ protons were shielded and detected clearly at δ_H 4.26–4.22 ppm and δ_H 1.29–1.26 ppm, respectively; for instance, methyl protons (**CH$_3$**–Ar) in **9** showed signal resonating at δ_H 2.41 ppm. ^{13}C-NMR spectrum confirmed the existence of amido and ester CO groups by showing signals at δ_C 171.9–163.5 ppm. The aromatic carbons resonated between δ_C 150.9–118.5 ppm. c-Hexylidene (O–**C**–CO) carbon signals ranged from δ_c 83.3–79.2 ppm. Also, cyclohexylidene carbon signals at δ_c 31.9–20.9 ppm. Signals were detected resonating at δ_C 61.0–60.5 ppm and δ_C 14.7–14.3 ppm for –OCH$_2$ and –CH$_3$ carbons, respectively. Carbons of the methyl group (**CH$_3$**–Ar) in product **9** showed signal resonating at δ_C 20.9 ppm. Also, product **13** showed a carbon signal at δ_C 44.4 ppm for methylene carbon (**CH$_2$**–NH).

Alternatively, Passerini reaction using **1** with trichloroacetic acid and cyclohexanone proceeded to afford the unexpected
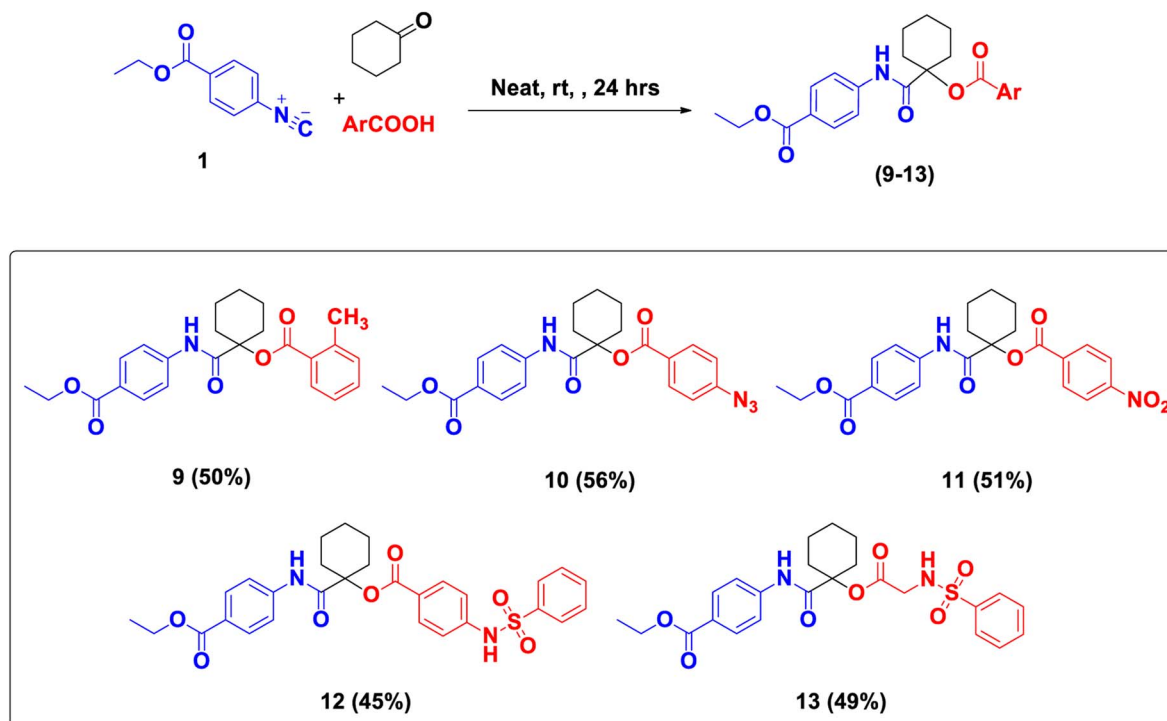
Scheme 3 Synthesis of α-acyloxy carboxamide derivatives **9–13** via Passerini reaction.
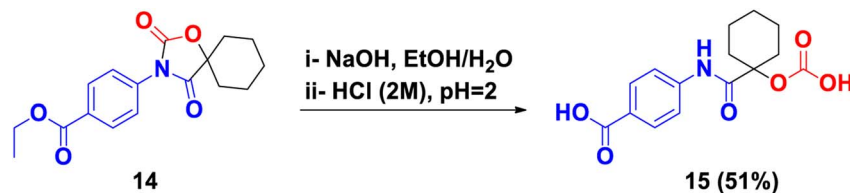
Scheme 4 Synthesis of 4-(1-(carboxyoxy)cyclohexane-1-carboxamido)benzoic acid **15**.

Passerini adduct ethyl 4-(2,4-dioxo-1-oxa-3-azaspiro[4.5]decan-3-yl)benzoate **14**.[62] Saponification of **14** in NaOH followed by acidification led to the formation of 4-(1-(carboxyoxy)cyclohexane-1-carboxamido)benzoic acid **15** (Scheme 4). The obtained monocarbonate ester **15** was confirmed by ^{1}H-NMR spectroscopy where two carboxylic protons showed a signal at δ_H 12.66 ppm and one proton of –NH at δ_H 10.04 ppm. ^{13}C-NMR spectrum recorded signals at δ_C 173.9 and 167.0 ppm, corresponding to NH–CO and Ar–CO–OH carbons, respectively. The carbon signal of O–CO–OH resonated at δ_C 152.1 ppm, while the carbon signals of O=C–CO appeared at δ_c 79.2 ppm.

Moreover, hydrazinolysis of **11** by reflux with hydrazine afforded N-(4-(hydrazinecarbonyl)phenyl)-1-hydroxycyclohexane-1-carboxamide (**16**), which upon treatment with phenylisothiocyanate (PhNCS) afforded 1-hydroxy-N-(4-(2-(phenylcarbamothioyl)hydrazine-1-carbonyl)phenyl)cyclohexane-1-carboxamide (**17**) (Scheme 5). The products **16** and **17** were confirmed by ^{1}H-NMR spectroscopy. With respect to **16**, its ^{1}H-NMR recorded three isolated signals at δ_H 9.76, 9.61, and 7.22 ppm, representing 3-NH protons and another signal at δ_H 5.49 ppm for the OH group. ^{13}C-NMR spectrum recorded signals resonating at δ_C 176.9 and 167.9 ppm, corresponding to carbons of two NH–CO groups. Also, the signal was detected for carbon in the O=C–C–OH group at δ_c 74.4 ppm. On the other hand, the disubstituted semicarbazide **17** showed four signals at δ_H: 10.39, 9.86, 9.76, and 9.65 ppm, corresponding to 4 NH. Also, another singlet appeared at δ_H 5.51 ppm, equivalent to the quaternary OH group. ^{13}C-NMR spectrum of **17** recorded two carbon signals at δ_C 177.0 and 166.0 ppm, corresponding to two carbons of 2 NH–CO. Also, the signal was detected for carbon in the O=C–C–OH group at δ_C 74.5 ppm.

4.2. Biological evaluation

4.2.1. Cytotoxicity screening. Cytotoxic effects of fourteen new target adducts were evaluated on breast cancer cell lines (MCF-7 and MDA-MB 231) and normal fibroblast cell line (WI-38) utilizing the microculture MTT method.[64] All test compounds have high IC$_{50}$–N values ($\geq$0.5 μM) except compounds **2** and **4**, which clarifies their selectivity on the breast cancer cells, in addition to their potential EC$_{100s}$. Most of them displayed preferential potent cytotoxic effects against MCF-7. The target compounds, **4**, **8**, and **12**, exhibited the strongest antiproliferative activity against both MCF-7 (IC$_{50}$ = 0.065–0.096 μM) and MDA-MB 231 cells (IC$_{50}$ = 0.135–0.188 μM). Meanwhile, compounds **3** and **17** showed preferential cytotoxicity against MCF-7 cells with IC$_{50}$'s around 0.08 μM; however, they were less sensitive towards MDA-MB 231 cell lines (Table 1). Afterwards, all the promising compounds (**3**, **4**, **8**, **12** and **17**) were subjected to further mechanistic study on the breast cancer cell lines except compounds **3** and **17** (examined only on the MCF-7 cell line). Notably, most of our library demonstrated higher selectivity indices (1–18.7) towards the cancer cell lines compared to the reference drug, Doxorubicin (Dox. IC$_{50}$ = 0.56–0.09 μM) (Table 1).

4.2.2. P53 induction. P53 is the prime chaperone of the genome, which is adapted in more than fifty percent of tumors; its role halts cancer evolution. It regulates the transcription and arbitrates diverse biological activities like growing arrest and apoptosis. The outcomes disclosed that compounds **3**, **4**, **8**, **12**, and **17** markedly escalated P53 expressions in MCF-7 cell line by 4.1–5.1 fold changes, while in MDA-MB231 cells, compounds **4**, **8**, and **12** demonstrated enhancement of P53 by 3.3–4.3 fold changes compared to that of control causing hard move of the breast cancer cells regarding apoptosis (Table 2). It is worth mentioning that the P53 induction potential of the studied compounds in MCF-7 and MDA-MB 231 surpassed that of the reference doxorubicin (2.1 and 1.6 folds, respectively).

4.2.3. Evaluation of mitochondrial apoptosis regulators (BAX and Bcl-2). Conceivably, the apoptotic induction mechanism of P53 occurs by virtue of its part as dominant for the expression of target boosters, *e.g.*, the mitochondrial apoptosis regulators BAX, Bcl-2, p21, CDK$_2$, and PUMAα.[65] The B-cell lymphoma protein-2 (Bcl-2) families perform an imperative
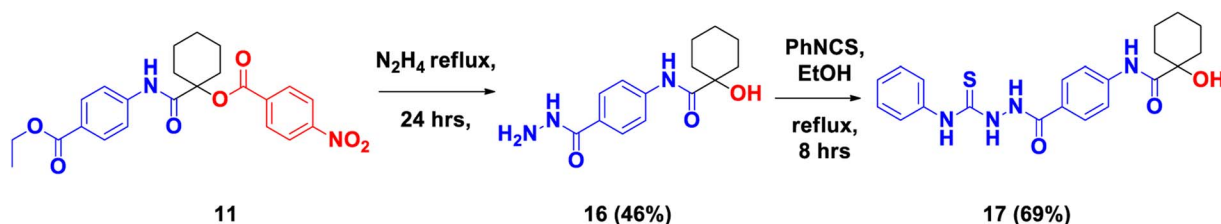

Scheme 5 Synthesis of the hydrazide **16** and thiosemicarbazide derivative **17**.

Table 1 Cytotoxicity and selectivity index (SI) values of the tested Ugi and Passerini adducts[a]

Compound no.	Wi-38		MCF-7		MDA-MB 231	
	IC$_{50}$ (μM)	EC$_{100}$ (μM)	IC$_{50}$ (μM)	SI	IC$_{50}$ (μM)	SI
2	0.147 ± 0.020	0.024 ± 0.004	0.369 ± 0.014	0.398	0.472 ± 0.013	0.311
3	**1.329 ± 0.084**	**0.302 ± 0.064**	**0.086 ± 0.016**	**15.453**	**0.306 ± 0.014**	**4.343**
4	**0.418 ± 0.033**	**0.141 ± 0.018**	**0.096 ± 0.007**	**4.354**	**0.188 ± 0.044**	**2.223**
5	0.570 ± 0.072	0.197 ± 0.006	0.229 ± 0.042	2.489	0.302 ± 0.024	1.887
6	0.538 ± 0.025	0.172 ± 0.009	0.143 ± 0.016	3.762	0.370 ± 0.094	1.454
8	**0.953 ± 0.037**	**0.376 ± 0.004**	**0.078 ± 0.072**	**12.217**	**0.146 ± 0.034**	**6.527**
9	0.608 ± 0.012	0.133 ± 0.013	0.440 ± 0.006	1.382	0.445 ± 0.004	1.366
10	0.505 ± 0.001	0.242 ± 0.031	0.439 ± 0.005	1.150	0.470 ± 0.012	1.074
11	0.516 ± 0.011	0.110 ± 0.013	0.591 ± 0.035	0.873	0.756 ± 0.175	0.683
12	**0.633 ± 0.001**	**0.208 ± 0.003**	**0.065 ± 0.050**	**9.738**	**0.135 ± 0.000**	**4.689**
13	0.590 ± 0.026	0.147 ± 0.028	0.142 ± 0.027	4.155	0.513 ± 0.066	1.150
15	0.827 ± 0.004	0.200 ± 0.028	0.264 ± 0.159	3.133	0.261 ± 0.025	3.169
16	3.327 ± 0.032	1.194 ± 0.020	0.968 ± 0.036	3.437	1.028 ± 0.036	3.236
17	**1.535 ± 0.122**	**0.466 ± 0.070**	**0.082 ± 0.002**	**18.720**	**0.518 ± 0.081**	**2.963**
Dox.	0.272 ± 0.053	0.074 ± 0.008	0.478 ± 0.076	0.569	2.828 ± 0.173	0.096

[a] Values are demonstrated as mean ± SEM.

Table 2 Relative fold change in the P53 expression in the treated breast cancer cells[a]

Compound no.	MCF-7	MDA-MB 231
3	4.110 ± 0.1014	ND
4	4.137 ± 0.0407	3.309 ± 0.110
8	4.810 ± 0.1014	3.733 ± 0.023
12	5.168 ± 0.0676	4.312 ± 0.075
17	4.377 ± 0.144	ND
Doxorubicin	2.148 ± 0.174	1.623 ± 0.122

[a] Values are demonstrated as mean ± SEM.

function in cancer advancement or reticence of the intrinsic apoptotic path provoked by a disorder of mitochondria, with Bcl-2 itself and pro-apoptotic proteins including BAX.[66] Considerable BAX sensitizers have been recognized as selective cancer remedies with the assets of selectivity and the potential to overcome resistance generated by chemicals and radiation. Possibly, Bcl-2 levels may decline if BAX ranks in the mitochondria are to elevate. The result of the promising Ugi and Passerine adducts (3, 4, 8, 12, and 17) on the expression rank of

BAX and Bcl-2 was evaluated. Conclusively, all our apoptotic inducer hits (3, 4, 8, 12, and 17) brought about overexpression of apoptosis regulator BAX by 2.3–3.3 folds. On the other hand, it greatly diminished the antiapoptotic levels of oncogenes, Bcl-2, by 0.13–0.49 folds in the tested cancer cell lines, MCF-7 and MDA-MB 231. Certainly, there is solid evidence that the correlation of BAX *versus* Bcl-2 proteins is a good indicator of the propensity of cancer cells to go through apoptosis precisely[67] (Table 3). Further experiments revealed that the studied compounds were superior to doxorubicin regarding the relative fold increment in BAX and decrement in Bcl-2 of both cell lines, except for 3 and 17 in MDA-MB 231 cells (Table 3).

4.2.4. Evaluation of caspase 3/7. Mechanistic study of apoptotic enhancement by the promising MTT assay hits (3, 4, 8, 12 and 17) was evaluated by calculating caspase 3/7 activation[68] percentages in breast cancer cell lines. These cell lines were treated with IC$_{50}$s of the investigated compounds. Analysis revealed that 3, 4, 8, 12 and 17 could induce the activation of caspase 3/7 by 2.6–4.1 folds in the treated breast cancer cell lines even more than doxorubicin, except for 3 and 17 in MDA-MB 231 cells. Impressively, compound 12 displayed the top caspase 3/7 fold activation (Table 4).

Table 3 Relative fold changes in BAX and Bcl-2 expression in the treated breast cancer cells[a]

Compound no.	MCF-7		MDA-MB 231	
	BAX	Bcl-2	BAX	Bcl-2
3	2.448 ± 0.057	0.217 ± 0.006	ND	ND
4	2.747 ± 0.1285	0.233 ± 0.0017	2.338 ± 0.021	0.496 ± 0.005
8	3.195 ± 0.082	0.163 ± 0.0035	2.479 ± 0.030	0.454 ± 0.010
12	3.337 ± 0.1485	0.129 ± 0.0027	2.683 ± 0.065	0.376 ± 0.037
17	3.042 ± 0.0365	0.201 ± 0.0075	ND	ND
Doxorubicin	1.556 ± 0.054	0.592 ± 0.031	1.232 ± 0.019	0.798 ± 0.044

[a] Values are demonstrated as mean ± SEM.

Table 4 Relative fold activation of caspase 3/7 in the treated breast cancer cells[a]

Compound no.	MCF-7	MDA-MB 231
3	**3.470** ± 0.0485	ND
4	**3.113** ± 0.10115	2.618 ± 0.1615
8	**3.763** ± 0.011	2.945 ± 0.0885
12	**4.105** ± 0.0795	3.304 ± 0.0745
17	**3.677** ± 0.0145	ND
Doxorubicin	**1.881** ± 0.028	1.272 ± 0.074

[a] ND: not done; values are demonstrated as mean ± SEM.

Fig. 3 Apoptotic cell population (%) in the treated breast cancer lines.
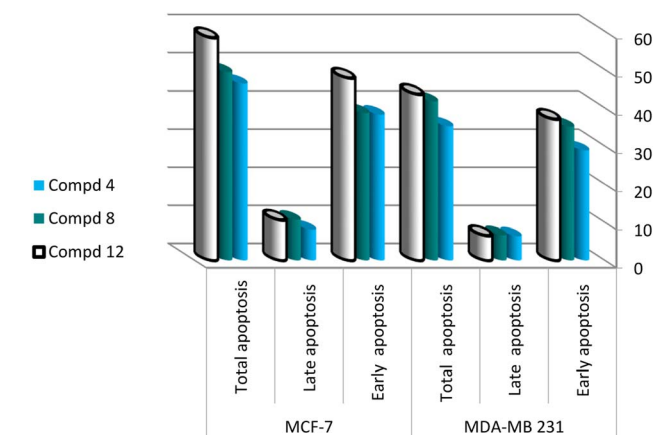
4.2.5. Morphological investigation of the enhanced apoptosis. The most selective and potent cytotoxic agents **4**, **8** and **12** were selected for morphological analysis of any changes that occur upon treatment with the breast cancer cell lines, MCF-7 and MDA-MB 231 correlated to the untreated cancer cells (Fig. 2). Obviously, all the treated cells missed their original architectures. Furthermore, extreme shrinking appeared for the designated dominant anti-breast cancer activities of our MTT assay hits, particularly **8** compared to that of the untreated cancer cells.

4.2.6. Flow cytometry for apoptosis detection.[69] To confirm apoptotic induction of compounds **4**, **8** and **12**, Annexin V-FITC and propidium iodide (PI) double staining by flow cytometer was carried out in MCF-7 and MDA-MB 231 cells treated with IC_{50}s of selected compounds for 72 h. Results clarified powerful apoptotic activation potential as demonstrated by a significant proportion of the total apoptotic cell population, 58.33%, 49.36%, and 45.34%, for compounds **12**, **8** and **4**, respectively, in the treated cells, as shown in Fig. 3 and 4. Accordingly, these results were concordant with that of the caspase 3/7 activation assay.

4.3. Molecular modeling studies

4.3.1. Docking simulations

4.3.1.1. Binding mode analysis of the caspase 3/7 activator hits into XIAP BIR2 domain. Based on our design strategy, the binding mode of the hit compounds into XIAP, the SMAC mimetics molecular target (Fig. 1; I & II), was explored. XIAP

functions as an apoptosis inhibitor through direct binding to BIR domains. It is known that the BIR2 domain inhibits caspase 3 and 7,[10,70–74] whereas the BIR3 domain selectively targets caspase 9. Various structure-based studies reported that SMAC mimetics that can bind into the XIAP BIR domains directly antagonize the inhibitory potential of XIAP against caspase, thus inducing apoptosis[75–78] Herein, docking of the hit caspase activators was simulated within the XIAP BIR2 domain that selectively binds caspase 3/7 employing MOE 2019.102.[79] The crystal structure of the XIAP BIR2 domain complexed with a benzodiazepinone-based inhibitor was retrieved from the protein data bank (PDB ID: 4KJU)[80] (Fig. 5). After default structure preparation, the studied compounds were built *in silico*, energy minimized, and docked into the ligand binding site of XIAP BIR2 domain. The docking protocol was preliminarily validated by redocking the reference ligand ($\Delta G = -8.66$ kcal mol^{-1}) with restoration of nearly all the experimental interactions (Fig. 5, panels K and L). The most potent caspase activator **12** fitted well into the ligand's site within the BIR2 domain, recording the most favored free binding energy ($\Delta G = -7.16$ kcal mol^{-1}) among the group (Table 5). The aromatic rings encompassing the sulphonamide group interacted with Leu207 and Asp214 *via* π–H and hydrogen bonds resembling
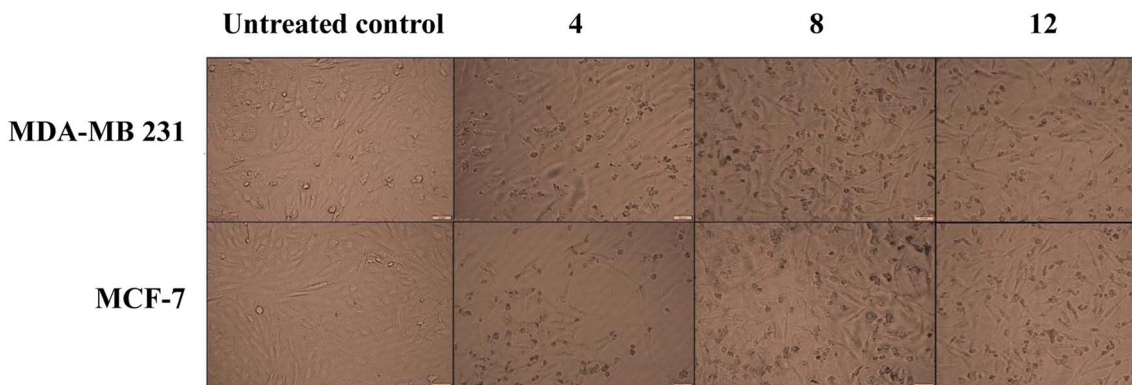
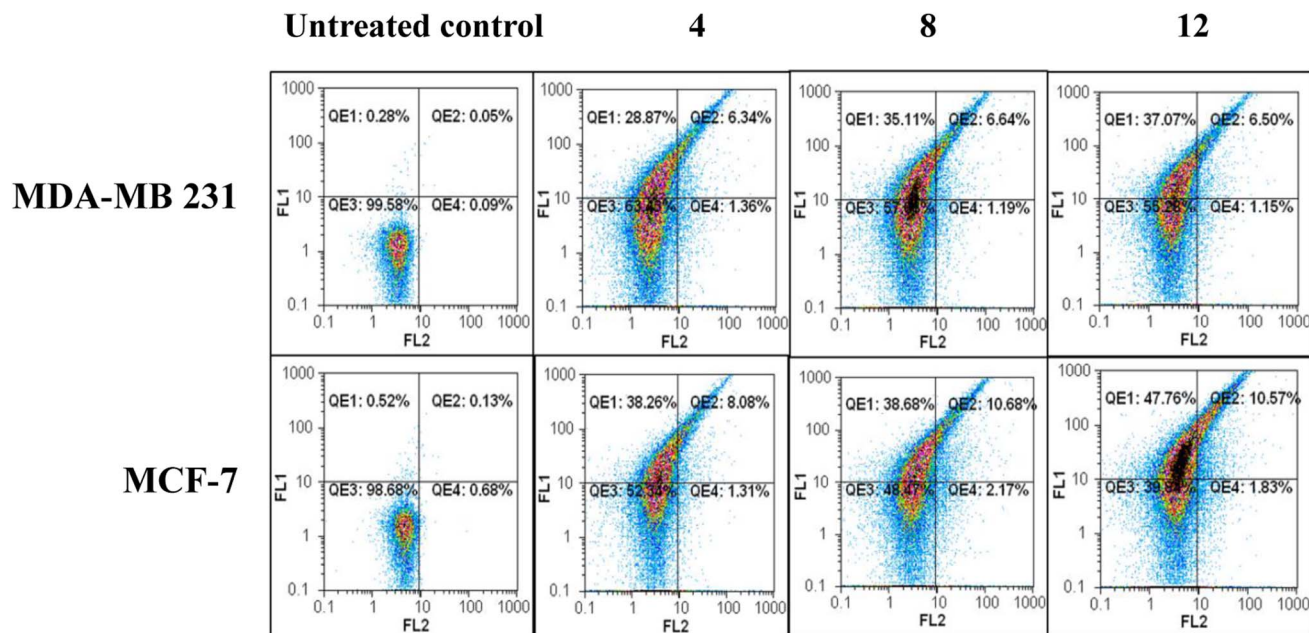**Fig. 2** Morphological changes of breast cancer cells after 72 h treatment with the promising hits.

Fig. 4 Flow charts of annexin-PI analysis of 4, 8 and 12-treated breast cancer cell lines.

the reference inhibitor in addition to H-bonds linking the amide and terminal ester carbonyl oxygens of the scaffold with Lys206 and Arg156 (Fig. 5, panels G and H). The cyclized derivative **8** displayed π–H and hydrogen bond interactions with the ligand essential residues Leu207, Ly208, and His223, besides the nearby Lys206 (Fig. 5, panels E and F). The thiosemicarbazide motif in **17** interacted with Asp214 and Arg222 through hydrogen bonds, whereas the backbone phenyl ring exhibited H–π interactions with Lys208 (Fig. 5, panels I and J). The Ugi adduct **3** also shared interactions with Lys208, Arg222, and His223 (Fig. 5, panels A and B). The iodophenyl analog **4** displayed multiple H–π interactions with Lys208, Trp210, and Phe224 (Fig. 5, panels C and D).

Herein, it could be assumed that the compounds could bind to the XIAP BIR2 domain, the molecular target of SMAC mimetics caspase 3/7 activators. Interestingly, these results could be correlated to the *in vitro* caspase 3/7 activation assay results, highlighting the main pharmacophoric features of the studied compounds. The cyclization of Ugi scaffold in future studies, given their expected key interactions with the BIR2 domain, should be specially considered.

4.3.1.2. Binding mode analysis of the P53 activator hits into MDM2. The E3 ubiquitin-protein ligase MDM2 crystal structure was retrieved from the protein databank co-crystallized with the reference inhibitor spiro[3H-indole-3,2′-pyrrolidin]-2(1H)-one **6SJ** (PBD ID: 5LAW[82]). The protein was prepared, employing MOE "QuickPrep" module after eliminating unwanted residues. The studied derivatives (Table 6) were built *in silico* and energy minimized, then docked into the co-crystallized ligand's binding site after validating the adopted protocol (Fig. 6). The best simulated binding modes (Fig. 6) showed that the hit compounds were able to reside well in the ligand's site with free

binding energies (Table 6) comparable to the redocked reference inhibitor **6SJ** ($\Delta G = -8.40$ kcal mol^{-1}) while sharing some essential interactions (Fig. 6, panels K and L). Interestingly, the most active Passerini-derived P53 inducer **12** recorded the most favorable free binding energies among the group ($\Delta G = -6.93$ kcal mol^{-1}), displaying π–π interactions between the terminal phenyl group and His96$_{(MDM2)}$ in the Leu26$_{(P53)}$ pocket (Fig. 6, panels G and H). The less active tolyl **3** and iodo **4** Ugi derivatives showed similar π–π interactions at less favored free binding energies ($\Delta G = -6.91$ and -6.73 kcal mol^{-1}) (Fig. 6, panels A–D). The cyclic analog **8** ($\Delta G = -6.80$ kcal mol^{-1}) was buried into the Trp23$_{(P53)}$ and Phe19$_{(P53)}$ pockets, forming H–π and hydrogen bond interactions with Leu54$_{(MDM2)}$ and Lys94$_{(MDM2)}$, respectively, as the reference **6SJ** (Fig. 6, panels E and F). Similarly, the thiosemicarbazide derivative **17** ($\Delta G = -6.28$ kcal mol^{-1}) exhibited similar interactions with additional hydrogen bonding between the terminal alcoholic group and Glu69 (Fig. 6, panels I and J). Considering these observations, it could be postulated that the studied derivatives share some predicted key interactions with the reference inhibitor. The molecular modeling results could be nearly correlated to the P53 induction results (Table 6).

4.3.2. In silico prediction of physicochemical characters and drug-like properties. We applied different computational procedures to appraise whether our small molecules acquire the ideal physicochemical and drug-like parameters. Molinspiration[83] software was utilized for prediction of descriptors from Lipinski's rule of five,[84] which considers that cell permeability and oral bioavailability are feasible if at least three rules are fulfilled. Appropriately, Lipinski's factors may be estimated. Oral bioavailability as a valuable descriptor of drug candidates[85] can be concluded from the topological polar surface area
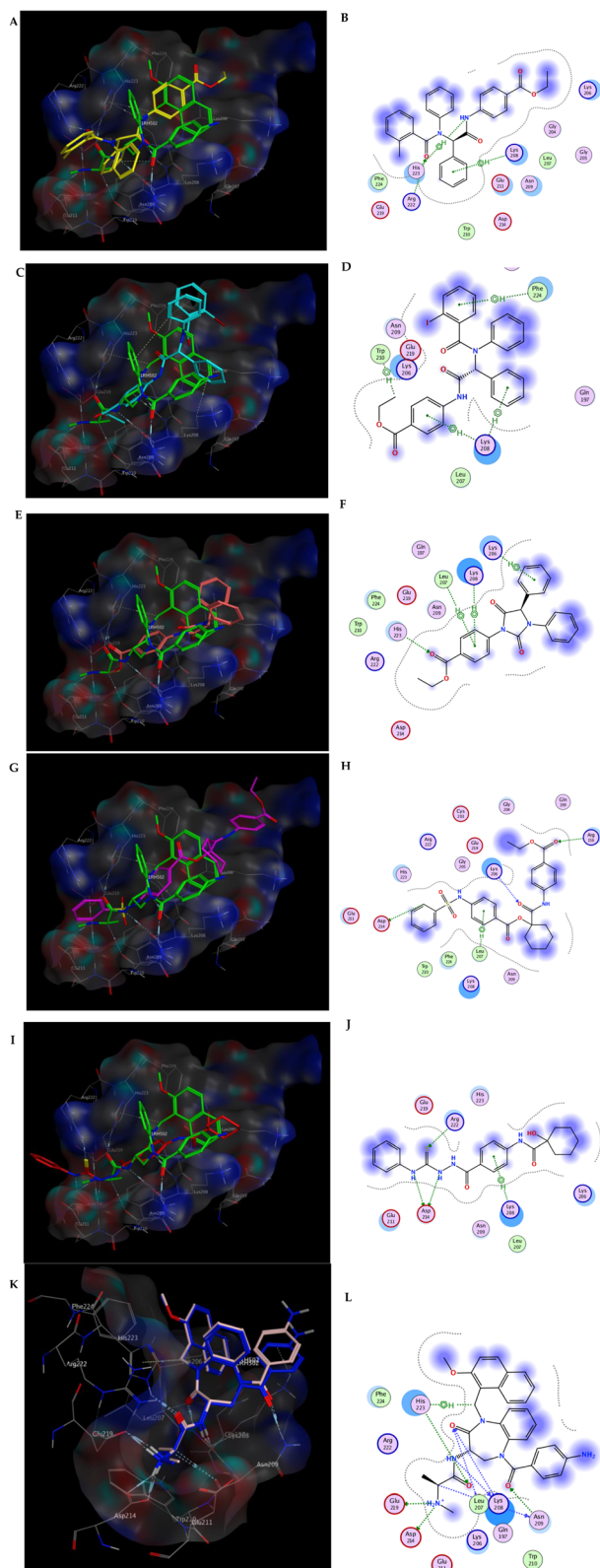
Fig. 5 (A) Overlay of the 3D binding mode of the co-crystallized ligand (green sticks) and **3** (yellow sticks), (B) 2D binding mode of **3**, (C) overlay of the 3D binding mode of the co-crystallized ligand (green sticks) and **4** (cyan sticks), (D) 2D binding mode of **4**, (E) overlay of the 3D binding mode of the co-crystallized ligand (green sticks) and **8** (pink sticks), (F) 2D binding mode of **8**, (G) overlay of the 3D binding mode of the co-crystallized ligand (green sticks) and **12** (magenta sticks), (H) 2D binding mode of **12** (I) overlay of the 3D binding mode of the co-crystallized ligand (green sticks) and **17** (red sticks), (J) 2D binding mode of **17** into the XIAP BIR2 domain (PDB ID: 4KJU[80,81]), (K) superposition of the modeled (blue sticks) and the co-crystallized benzodiazepinone inhibitor (light pink sticks), and (L) 2D binding mode of the co-crystallized inhibitor in the XIAP BIR2 domain (PDB ID: 4KJU[80,81]).

Table 5 The ligand−receptor complex binding free energies ΔG (kcal mol^{-1}) of the docked caspase 3/7 activator hits into the XIAP BIR2 domain

Compound no.	ΔG (kcal mol^{-1})
3	−6.30
4	−6.53
8	−6.19
12	−7.16
17	−6.60
Co-crystallized inhibitor	−8.66

Table 6 The ligand−receptor complex binding free energies ΔG (kcal mol^{-1}) of the P53 activator hits into MDM2

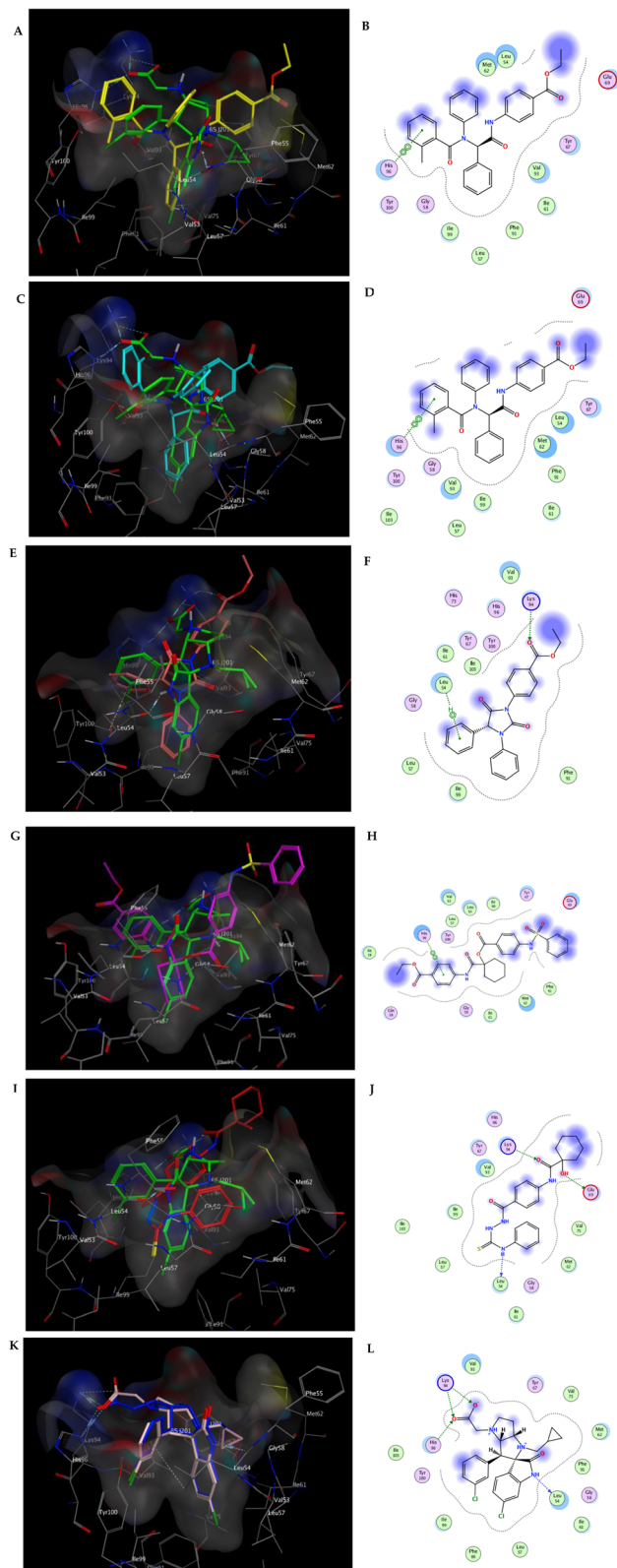| Compound no.	ΔG (kcal mol^{-1})
3	−6.91
4	−6.72
8	−6.80
12	−6.93
17	−6.28
6SJ	−8.40

(TPSA)[86,87] and the number of rotatable bonds (NROTB). Grounded on TPSA following the equation: ABS (%) = 109−0.345TPSA, the absorption percentage could also be predicted. Subsequently, *in silico* physicochemical characters of the new compounds were determined (Table 7). Interestingly, all compounds, except **6** (3 violations), were in complete agreement with Lipinski's rule of five. Compounds **2–6** and **9–12** exhibited modest infractions concerning log *P*, while compounds **4–6** and **12** demonstrated violations of Lipinski's rule concerning molecular weight (MWt). All compounds except **6** were in the reasonable range for TPSA values. As a consequence, the majority of our compounds elicited acceptable %ABS ranging from 51.26–85.91%, suggesting promising cell permeability and oral bioavailability.

Moreover, Swiss ADME software[88] was applied to predict drug-like and medical chemistry characteristics of the test compounds, as described in Table 8. All compounds showed high bioavailability scores (0.55) except compounds **4** and **6**, with a bioavailability score of 0.17. Besides, no alerts are predicted for all compounds except **10** (containing the N$_3$ group). Overall, it could be established that the promising compounds presented acceptable physicochemical values as well as drug-like characteristics, which may introduce them as promising drug-like compounds.

5. Structure–activity relationship

Generally, the activity motif proposes that the bisamide-based scaffold preserved the intrinsic antitumor activity of the reported lead apoptotic inducers (Fig. 1). Concerning the cytotoxicity of the Ugi adducts (**2–6**, **8**) towards the two cancer breast cell lines, the activity profile demonstrated higher potency against MCF-7 than MDA-MB 231. On examining the effect of substituents on the adduct activities, results showed that the derivative **4** bearing 2-iodophenyl was more potent, particularly against MDA-MB 231 ($IC_{50} = 0.188$ μM) than its analog, **3** bearing 2-tolyl group ($IC_{50} = 0.306$ μM). The influence of the substituent effect on the observed cytotoxic profile of the scaffold was also deduced by introducing 2-nitrophenyl or 3,5-dinitrophenyl groups to the Ugi adducts **5** and **6**, respectively. Herein, the 2-nitrophenyl derivative **5** was less potent and selective than the 2-iodophenyl **4** and the 2-methylphenyl **3** derivatives. The 3,5-dinitrophenyl analog **6** showed a supplemental increase in potency and selectivity relative to the 2-nitrophenyl derivative, however, still less active than the 2-idophenyl derivative. The notable potency of the iodophenyl derivative **4** may be attributed to the possibility of halogen bonding with the target receptors. Based on previous studies, interactions between C–I and oxygen of carbonyl, hydroxyl, charged carboxylate, or phosphate group (OY) in biological receptors (C–I···OY) potentially stabilize inter- and intramolecular interactions that can affect ligand binding and molecular folding where the I···O distance is less than or equal to the sums of the respective Van der Waals radii.[89,90]

Deletion of the phenyl group and introduction of a trifluoromethyl group in compound **2** was detrimental to the scaffold's selectivity. Obviously, rigidification of the intermediate **7** furnished the imidazolidindione **8** with remarkable cytotoxicities against both MCF-7 ($IC_{50} = 0.078$ μM) and MDA-MB 231 ($IC_{50} = 0.146$ μM). When comparing the cytotoxic results of Ugi adduct, **3** (IC_{50} 0.086) and its isostere, Passerini adduct, **9** ($IC_{50} = 0.44$ μM) on MCF-7 cell line, remarkable cytotoxicity of **3** carrying phenyl can be attributed to its higher lipophilic character than **9**, which bears a cyclohexylidene moiety. Notably, compound **12** bearing central phenyl exhibited superior activity on both cell lines than its counterpart **13**, which bears methylene spacer instead; for instance, on the MCF-7 cell line, **12** elicited $IC_{50} = 0.065$ μM while **13** demonstrated $IC_{50} = 0.142$ μM. This emphasizes the importance of lipophilicity for the cytotoxic activity of our studied compounds. Moreover, extension strategy on the acid hydrazide, **16** (MCF-7, $IC_{50} = 0.968$ μM) and (MDA-MB 231, $IC_{50} = 1.028$ μM) gave compound **17** with escalated anticancer activity towards both MCF-7s ($IC_{50} = 0.082$ μM) and MDA-MB 231 ($IC_{50} = 0.518$ μM).

Fig. 6 (A) Overlay of the 3D binding mode of the co-crystallized ligand (green sticks) and **3** (yellow sticks), (B) 2D binding mode of **3**, (C) overlay of the 3D binding mode of the co-crystallized ligand (green sticks) and **4** (cyan sticks), (D) 2D binding mode of **4**, (E) overlay of the 3D binding mode of the co-crystallized ligand (green sticks) and **8** (pink sticks), (F) 2D binding mode of **8**, (G) overlay of the 3D binding mode of the co-crystallized ligand (green sticks) and **12** (magenta sticks), (H) 2D binding mode of **12** (I) overlay of the 3D binding mode of the co-crystallized ligand (green sticks) and **17** (red sticks), (J) 2D binding mode of **17** into the co-crystallized inhibitor 6SJ binding site (PBD ID: 5LAW).[82] (K) Superposition of the modeled (blue sticks) and the co-crystallized benzodiazepinone inhibitor (light pink sticks), and (L) 2D binding mode of the co-crystallized inhibitor in the MDM2 (PBD ID: 5LAW).[82]

Table 7 *In silico* prediction of physicochemical properties of all compounds

Compound no.	Log P	MWt	HBA[a]	HBD[b]	Lipinski's violation	TPSA	ABS (%)	Volume (A³)	NROTB
2	5.22	470.45	6	1	1	75.71	82.88	399.47	9
3	6.41	492.57	6	1	1	75.71	82.88	456.14	9
4	7.04	604.44	6	1	2	75.71	82.88	463.57	9
5	5.92	523.54	9	1	2	121.54	67.07	462.92	10
6	5.85	568.54	12	1	3	167.36	51.26	486.25	11
8	4.94	400.43	6	0	0	66.92	85.91	357.71	6
9	5.50	409.48	6	1	1	81.71	80.81	382.37	8
10	6.48	436.47	9	1	1	131.46	63.65	390.70	9
11	5.39	440.45	9	1	1	127.53	65.00	389.14	9
12	6.20	550.63	9	2	2	127.88	64.88	481.05	11
13	4.19	488.56	9	2	0	127.88	64.88	426.24	11
15	2.22	307.30	7	3	0	112.93	70.04	268.09	5
16	0.84	277.32	6	5	0	104.45	72.96	255.79	3
17	2.66	412.51	7	5	0	102.48	73.64	368.58	7

[a] HBA: number of hydrogen bond acceptors. [b] HBD: number of hydrogen bond donors.

Table 8 Drug-like and medicinal chemistry parameters

Compound no.	Bioavailability score	PAINS	Synthetic accessibility
2	0.55	0	3.29
3	0.55	0	3.63
4	0.17	0	3.69
5	0.55	0	3.91
6	0.17	0	4.07
8	0.55	0	3.23
9	0.55	0	2.95
10	0.55	1	3.12
11	0.55	0	3.04
12	0.55	0	3.64
13	0.55	0	3.55
15	0.56	0	2.24
16	0.55	0	1.86
17	0.55	0	3.03

Among all tested compounds, compound **12** elicited the highest cytotoxicity against both types of breast cancer.

6. Conclusions

The current study reports a quick mechanistic investigation of the apoptotic induction potential of rationally designed flexible and constrained Passerini and Ugi derivatives. The promising adducts **3**, **4**, and **12**, the cyclized imidazolidine derivative **8**, as well as the thiosemicarbazide derivative **17** exhibited selective cytotoxic activity against breast cancer cell line (MCF-7, MDA-MB231) activated caspase 3/7 by 3.1–4.1 folds and promoted increased P53 signaling by 4.1–5.1 fold changes in MCF-7 cells line. Among the group, only **4**, **8** and **12** demonstrated dual activities in MDA-MB231 cells. Further mechanistic studies showed that the compounds induced overexpression of BAX and downregulated the antiapoptotic oncogene, Bcl-2. Docking studies aided by SAR studies and ADME calculations indicated their acceptable pharmacokinetics and drug-like properties.

Conflicts of interest

The authors declare no conflict of interest.

Acknowledgements

References

1 L. Yuan, Y. Cai, L. Zhang, S. Liu, P. Li and X. Li, *Front. Pharmacol*, 2021, **12**, 1–45.
2 O. Yersal and S. Barutca, *World J. Clin. Onco.*, 2014, **5**, 412.
3 I. Tsaur, I. Heidegger, A. Kretschmer, H. Borgmann, G. Gandaglia, A. Briganti, P. De Visschere, R. Mathieu, M. Valerio and R. van den Bergh, *Cancer Treat. Rev.*, 2019, **75**, 20–26.
4 K.-S. H. Nguyen, J. W. Neal and H. Wakelee, *World J. Clin. Onco.*, 2014, **5**, 576.
5 C. M. Neophytou, I. P. Trougakos, N. Erin and P. Papageorgis, *Cancers*, 2021, **13**, 4363.
6 R. Siegel, K. Miller and A. Jemal, *Am. Cancer Soc.*, 2020, **70**, 7–30.
7 Z. Kozovska, V. Gabrisova and L. Kucerova, *Biomed. Pharmacother.*, 2014, **68**, 911–916.
8 R. Rathore, J. E. McCallum, E. Varghese, A.-M. Florea and D. Büsselberg, *Apoptosis*, 2017, **22**, 898–919.
9 S. Fulda, *Clin. Cancer Res.*, 2014, **20**, 3915–3920.
10 Q. L. Deveraux and J. C. Reed, *Genes Dev.*, 1999, **13**, 239–252.
11 A. Dey, V. Tergaonkar and D. P. Lane, *Nat. Rev. Drug Discovery*, 2008, **7**, 1031–1040.
12 P. Ak and A. J. Levine, *Faseb J.*, 2010, **24**, 3643–3652.
13 T. Liu, L. Zhang, D. Joo and S.-C. Sun, *Signal Transduction Targeted Ther.*, 2017, **2**, 1–9.
14 T. Scholzen and J. Gerdes, *J. Cell. Physiol.*, 2000, **182**, 311–322.

15 E. C. Kauffman, V. L. Robinson, W. M. Stadler, M. H. Sokoloff and C. W. Rinker-Schaeffer, *J. Urol.*, 2003, **169**, 1122–1133.

16 A. Beloglazkina, N. Zyk, A. Majouga and E. Beloglazkina, *Molecules*, 2020, **25**, 1211.

17 C. Riedinger and J. M. McDonnell, *Future Med. Chem.*, 2009, **1**, 1075–1094.

18 M. Millard, D. Pathania, F. Grande, S. Xu and N. Neamati, *Curr. Pharm. Des.*, 2011, **17**, 536–559.

19 A. Barakat, M. S. Islam, H. M. Ghawas, A. M. Al-Majid, F. F. El-Senduny, F. A. Badria, Y. A. M. M. Elshaier and H. A. Ghabbour, *Bioorg. Chem.*, 2019, **86**, 598–608.

20 M. S. Islam, H. M. Ghawas, F. F. El-Senduny, A. M. Al-Majid, Y. A. M. M. Elshaier, F. A. Badria and A. Barakat, *Bioorg. Chem.*, 2019, **82**, 423–430.

21 G. Lotfy, Y. M. A. Aziz, M. M. Said, H. El Sayed, H. El Sayed, M. M. Abu-Serie, M. Teleb, A. Dömling and A. Barakat, *Bioorg. Chem.*, 2021, **117**, 105427.

22 Y. M. A. Aziz, G. Lotfy, M. M. Said, E. S. H. El Ashry, E. S. H. El Tamany, S. M. Soliman, M. M. Abu-Serie, M. Teleb, S. Yousuf and A. Dömling, *Front. Chem.*, 2021, **9**, 735236.

23 J. Li, J. Viallet and E. B. Haura, *Cancer Chemother. Pharmacol.*, 2008, **61**, 525–534.

24 V. Tergaonkar and N. D. Perkins, *Mol. Cell*, 2007, **26**, 158–159.

25 S. X. Cai, B. Nguyen, S. Jia, J. Herich, J. Guastella, S. Reddy, B. Tseng, J. Drewe and S. Kasibhatla, *J. Med. Chem.*, 2003, **46**, 2474–2481.

26 L. Bai, D. C. Smith and S. Wang, *Pharmacol. Ther.*, 2014, **144**, 82–95.

27 H. Sun, Z. Nikolovska-Coleska, C.-Y. Yang, D. Qian, J. Lu, S. Qiu, L. Bai, Y. Peng, Q. Cai and S. Wang, *Acc. Chem. Res.*, 2008, **41**, 1264–1277.

28 C. H. A. Cheung, Y.-C. Chang, T.-Y. Lin, S. M. Cheng and E. Leung, *J. Biomed. Sci.*, 2020, **27**, 1–10.

29 H. Cong, L. Xu, Y. Wu, Z. Qu, T. Bian, W. Zhang, C. Xing and C. Zhuang, *J. Med. Chem.*, 2019, **62**, 5750–5772.

30 P. Cetraro, J. Plaza-Diaz, A. MacKenzie and F. Abadía-Molina, *Cancers*, 2022, **14**, 1671.

31 M. Olsson and B. Zhivotovsky, *Cell Death Differ.*, 2011, **18**, 1441–1449.

32 T. K. Oost, C. Sun, R. C. Armstrong, A.-S. Al-Assaad, S. F. Betz, T. L. Deckwerth, H. Ding, S. W. Elmore, R. P. Meadows and E. T. Olejniczak, *J. Med. Chem.*, 2004, **47**, 4417–4426.

33 C. N. Johnson, J. S. Ahn, I. M. Buck, E. Chiarparin, J. E. H. Day, A. Hopkins, S. Howard, E. J. Lewis, V. Martins and A. Millemaggi, *J. Med. Chem.*, 2018, **61**, 7314–7329.

34 M. S. Ayoup, Y. Wahby, H. Abdel-Hamid, M. Teleb, M. M. Abu-Serie and A. Noby, *Eur. J. Med. Chem.*, 2019, **168**, 340–356.

35 Z. Mrkvová, S. Uldrijan, A. Pombinho, P. Bartůněk and I. Slaninová, *Molecules*, 2019, **24**, 2152.

36 L.-t. Wu, Z. Jiang, J.-j. Shen, H. Yi, Y.-c. Zhan, M.-q. Sha, Z. Wang, S.-t. Xue and Z.-r. Li, *Eur. J. Med. Chem.*, 2016, **114**, 328–336.

37 K. Błaszczak-Świątkiewicz, *Molecules*, 2019, **24**, 3902.

38 P. Boggu, E. Venkateswararao, M. Manickam, D. Kwak, Y. Kim and S.-H. Jung, *Bioorg. Med. Chem.*, 2016, **24**, 1872–1878.

39 P. Boggu, E. Venkateswararao, M. Manickam, Y. Kim and S.-H. Jung, *Arch. Pharmacal Res.*, 2017, **40**, 469–479.

40 K. J. Okolotowicz, R. Shi, X. Zheng, M. MacDonald, J. C. Reed and J. R. Cashman, *Bioorg. Med. Chem.*, 2010, **18**, 1918–1924.

41 G. Dunphy, S. M. Flannery, J. F. Almine, D. J. Connolly, C. Paulus, K. L. Jønsson, M. R. Jakobsen, M. M. Nevels, A. G. Bowie and L. Unterholzner, *Mol. Cell*, 2018, **71**, 745–760.

42 R. Poltz and M. Naumann, *BMC Syst. Biol.*, 2012, **6**, 1–19.

43 K. Jonak, M. Kurpas, K. Szoltysek, P. Janus, A. Abramowicz and K. Puszynski, *BMC Syst. Biol.*, 2016, **10**, 1–12.

44 M. Barani, M. Mirzaei, M. Torkzadeh-Mahani and M. Adeli-Sardou, *Sci. Rep.*, 2019, **9**, 7139.

45 M. Ríos-Gutiérrez, A. Barakat and L. R. Domingo, *Organics*, 2022, **3**, 122–136.

46 J. Araujo, E. Gonzalez-Mira, M. A. Egea, M. L. Garcia and E. B. Souto, *Int. J. Pharm.*, 2010, **393**, 168–176.

47 A. M. Al-Mahallawi, O. M. Khowessah and R. A. Shoukri, *Int. J. Pharm.*, 2017, **522**, 157–164.

48 H. Zhu, H. Gao, Y. Ji, Q. Zhou, Z. Du, L. Tian, Y. Jiang, K. Yao and Z. Zhou, *J. Hematol. Oncol.*, 2022, **15**, 91.

49 E. A. Mazyed and A. E. Abdelaziz, *Pharmaceutics*, 2020, **12**, 465.

50 S. T. Sp, M. Mothilal, N. Damodharan and D. Jaison, *Int. J. Appl. Pharm.*, 2018, 79–85.

51 M. S. Ayoup, A. F. Mansour, H. Abdel-Hamid, M. M. Abu-Serie, S. M. Mohyeldin and M. Teleb, *Eur. J. Med. Chem.*, 2023, **245**, 114865.

52 H. Liang, R. A. Salinas, B. Z. Leal, T. Kosakowska-Cholody, C. J. Michejda, S. J. Waters, T. S. Herman, J. M. Woynarowski and B. A. Woynarowska, *Mol. Cancer Ther.*, 2004, **3**, 1385–1396.

53 K. O. Mohamed, Y. M. Nissan, A. A. El-Malah, W. A. Ahmed, D. M. Ibrahim, T. M. Sakr and M. A. Motaleb, *Eur. J. Med. Chem.*, 2017, **135**, 424–433.

54 R. Ponce-Cusi and G. M. Calaf, *Int. J. Oncol.*, 2016, **48**, 774–782.

55 M. S. Ayoup, M. A. Fouad, H. Abdel-Hamid, M. M. Abu-Serie, A. Noby and M. Teleb, *Eur. J. Med. Chem.*, 2020, **186**, 111875.

56 P. S. Galatin and D. J. Abraham, *J. Med. Chem.*, 2004, **47**, 4163–4165.

57 Y. Wen, X. Chen, Z. Liu, Q. Zhu, Z. Li, G. He, H. Yan and Q. Lin, *ChemistrySelect*, 2021, **6**, 10965–10973.

58 L. Banfi, A. Basso, C. Lambruschini, L. Moni and R. Riva, *Chem. Heterocycl. Compd*, 2017, **53**, 382–408.

59 P. S. G. Nunes, H. D. A. Vidal and A. G. Corrêa, *Org. Biomol. Chem.*, 2020, **18**, 7751–7773.

60 J. G. Rudick, S. Shaabani and A. Dömling, *Front. Chem.*, 2020, **7**(918), 1–3.

61 M. Tandi and S. Sundriyal, *J. Indian Chem. Soc.*, 2021, **98**, 100106.

62 M. S. Ayoup, Y. Wahby, H. Abdel-Hamid, M. M. Abu-Serie and M. Teleb, *Sci. Rep.*, 2022, **12**, 22390.

63 X. Wang, Q.-G. Wang and Q.-L. Luo, *Synthesis*, 2015, **47**, 49–54.

64 T. Mosdam, *J. Immunol. Methods*, 1983, **65**, 55–63.

65 J. T. Zilfou and S. W. Lowe, *Cold Spring Harbor Perspect. Biol.*, 2009, **1**, a001883.

66 S. Fulda, L. Galluzzi and G. Kroemer, *Nat. Rev. Drug Discovery*, 2010, **9**, 447–464.

67 S. Salakou, D. Kardamakis, A. C. Tsamandas, V. Zolota, E. Apostolakis, V. Tzelepi, P. Papathanasopoulos, D. S. Bonikos, T. Papapetropoulos and T. Petsas, *In Vivo*, 2007, **21**, 123–132.

68 P. J. Lakshmi, B. S. Kumar, R. S. Nayana, M. S. Mohan, R. Bolligarla, S. K. Das, M. U. Bhanu, A. K. Kondapi and M. Ravikumar, *Bioorg. Med. Chem.*, 2009, **17**, 6040–6047.

69 Y. A. Ammar, A. M. S. El-Sharief, A. Belal, S. Y. Abbas, Y. A. Mohamed, A. B. Mehany and A. Ragab, *Eur. J. Med. Chem.*, 2018, **156**, 918–932.

70 G. S. Salvesen and C. S. Duckett, *Nat. Rev. Mol. Cell Biol.*, 2002, **3**, 401–410.

71 S. J. Riedl and Y. Shi, *Nat. Rev. Mol. Cell Biol.*, 2004, **5**, 897–907.

72 E. C. LaCasse, S. Baird, R. G. Korneluk and A. E. MacKenzie, *Oncogene*, 1998, **17**, 3247–3259.

73 M. Holcik, H. Gibson and R. G. Korneluk, *Apoptosis*, 2001, **6**, 253–261.

74 Y. Huang, Y. C. Park, R. L. Rich, D. Segal, D. G. Myszka and H. Wu, *Cell*, 2001, **104**, 781–790.

75 H. Sun, Z. Nikolovska-Coleska, J. Lu, S. Qiu, C.-Y. Yang, W. Gao, J. Meagher, J. Stuckey and S. Wang, *J. Med. Chem.*, 2006, **49**, 7916–7920.

76 H. Sun, J. A. Stuckey, Z. Nikolovska-Coleska, D. Qin, J. L. Meagher, S. Qiu, J. Lu, C.-Y. Yang, N. G. Saito and S. Wang, *J. Med. Chem.*, 2008, **51**, 7169–7180.

77 Y.-C. Chang and C. H. A. Cheung, *Appl. Sci.*, 2020, **11**, 335.

78 E. Morrish, G. Brumatti and J. Silke, *Cells*, 2020, **9**(406), 1–24.

79 *Molecular Operating Environment (MOE)*, 102 Chemical Computing Group ULC, Suite #910, 1010 Sherbooke St. West, 2R7, Canada, H3A, Montreal, QC, 2019, p. 2022.

80 R. F. Kester, A. F. Donnell, Y. Lou, S. W. Remiszewski, L. J. Lombardo, S. Chen, N. T. Le, J. Lo, J. A. Moliterni and X. Han, *J. Med. Chem.*, 2013, **56**, 7788–7803.

81 P. Andrews, D. Craik and J. Martin, *J. Med. Chem.*, 1984, **27**, 1648–1657.

82 M. H. Nematollahi, A. Pardakhty, M. Torkzadeh-Mahanai, M. Mehrabani and G. Asadikaram, *RSC Adv.*, 2017, **7**, 49463–49472.

83 *Molinspiration Cheminformatics*, August, 2023, https://www.molinspiration.com.

84 C. A. Lipinski, F. Lombardo, B. W. Dominy and P. J. Feeney, *Adv. Drug Delivery Rev.*, 1997, **23**, 3–25.

85 D. F. Veber, S. R. Johnson, H.-Y. Cheng, B. R. Smith, K. W. Ward and K. D. Kopple, *J. Med. Chem.*, 2002, **45**, 2615–2623.

86 P. Ertl, B. Rohde and P. Selzer, *J. Med. Chem.*, 2000, **43**, 3714–3717.

87 A. Polinsky and G. Shaw, *Pract. Med. Chem.*, 2003, 147–157.

88 A. Daina, O. Michielin and V. Zoete, *Sci. Rep.*, 2017, **7**, 1–13.

89 P. Auffinger, F. A. Hays, E. Westhof and P. S. Ho, *Proc. Natl. Acad. Sci.*, 2004, **101**, 16789–16794.

90 P. Metrangolo, H. Neukirch, T. Pilati and G. Resnati, *Acc. Chem. Res.*, 2005, **38**, 386–395.